THE MULTI-PASS DEFORMATION OF Ti-6Al-4V

Centre for Materials Engineering

Student: Bridget Gcinaphi Sikhondze

Supervisors: Dr. Sarah George and Prof. Robert Knutsen

A dissertation submitter to the Faculty of Engineering and the Built Environment

In fulfilment of the requirements for the degree of

Master of Science in Engineering

DECLARATION

I, Bridget Sikhondze, hereby declare that the work on which this thesis is based is my original work(except where acknowledgements indicate otherwise) and that neither the whole work nor any part of it has been, is being, or is to be submitted for another degree in this or any other university. I authorise the University to reproduce for the purpose of research either the whole or any portion of the contents in any manner whatsoever.

Signature…..Signed……..

Date……26/04/2017……

"You shoot me down but I won't fall, I am titanium."

David Guetta featuring Sia

Acknowledgements

My sincerest gratitude first and foremost goes to the National Research Foundation for funding this project. I would also like to express my thanks to the following people:

- My supervisor, Dr Sarah George, for her guidance, support and belief in me, even when things seemed very bleak.
- Professor Knutsen for his guidance.
- Dr Karine Kafer who "changed the game" as they say in hip hop. I am eternally grateful.
- My parents, Phetsani Manana and Mclean Sikhondze, as well as my eldest sibling, Phumlile Sikhondze, for supporting me financially.
- My sister Tsandzi Sikhondze for her moral support.
- Siboniso Mkhabela without whom I would not have gotten into UCT.
- Velile Vilane for his friendship, his readiness in sharing his valuable time giving insight on my project.
- Ryan Matthews for patiently teaching me how to use the SEM.
- Tyrone Newins for his aid with all things Gleeble.
- Penny Louw for her assistance in the lab, her generosity and snippets of advice.
- Colleagues and friends at CME for providing an excellent working environment.
- My friends in Swaziland who cheered me on from afar.
- Lastly, a Master's degree has so much to do with persistence and resilience. I would be remiss if I did not acknowledge myself for having both qualities.

Abstract

Ti-6Al-4V is a two-phase alloy used in the aerospace, military and biomedical industries. The thermomechanical processing (TMP) of Ti-6A-4V involves the breakdown of the ingot microstructure at temperatures above the beta transus (T_β) into fine lamellar colonies. Subsequent hot deformation is carried out at temperatures within the two-phase region to produce a microstructure that is either equiaxed or bimodal. However, to avoid the formation of shear bands, voids or cracks within the final microstructure, this secondary fabrication is carried out at slow speeds and these render the TMP of titanium a time-consuming and expensive process.

This project aims to investigate the possibility of using a steckel mill for the TMP of Ti-6Al-4V. A steckel mill is a single-stand reversing mill with two coiler furnaces on either side. These furnaces allow for the annealing of strip metal between passes, thus keeping the strip at a high temperature throughout processing. In this way, reversing passes can occur indefinitely until a desired gauge thickness is achieved. Therefore, a steckel mill represents a cheaper and faster method to produce metal sheet or plate.

Ti-6Al-4V cylinders with a diameter of 10mm and length of 15mm were uniaxially compressed in the Gleeble 3800. Hot compression was carried out isothermally in a three-pass schedule at temperatures of 850°C, 950°C and 1050°C respectively. The strain was kept constant at 0.48 and strain rates of 1/s and 10/s were employed. Interpass times corresponding to a strain rate of 10/s were 44s and 77s, while those corresponding to a strain rate of 1/s were 324s and 712s. Statistical analysis in the form of analysis of variance (ANOVA) was used to determine the parameter most influential on the microstructural evolution of Ti-6Al-4V.The Taguchi method was used to identify the optimum parameters suitable for the TMP of Ti-6Al-4V, using a steckel mill.

Three successive passes at 850°C, 1/s resulted in a microstructure consisting of coarse, deformed grains and some finer recrystallised grains. The influence of a low strain rate was such that it promoted recrystallisation at this temperature, while that of interpass time brought about recrystallisation and grain growth. At the same temperature and a strain rate of 10/s, less

recrystallisation, together with a heavily deformed microstructure, was observed. This was due to the heterogeneous distribution of strain, which was a consequence of the high strain rate used.

At 950°C, at both 1/s and 10/s, one pass resulted in a bimodal microstructure. With subsequent passes, the amount of equiaxed α was observed to increase. This increase was a result of a strain-induced transformation (SIT) from (β) to (α) phase at high temperatures. The extent of this transformation increased with an increase in strain rate. Therefore, after three consecutive passes at 10/s, a fully α (though heavily deformed) microstructure was formed. A subsequent post-deformation heat treatment would lead to recrystallisation of these grains and a microstructure consisting of refined equiaxed α grains was the result.

After one pass at 1050°C, at either 1/s or 10/s, a Widmanstätten microstructure was formed. However, after three consecutive passes at 1/s, the microstructure remained mostly Widmanstätten, while at 10/s, a bimodal microstructure was formed. The combination of a high strain rate, low interpass times and sequential strain imparted on the sample, as well as the high temperature at which the compressions were carried out, elevated the extent to which a strain-induced phase transformation from β to α proceeded.

Statistical analysis using ANOVA and the Taguchi method revealed that a schedule of three passes performed at 1050°C, 1/s and the corresponding interpass times were the optimum parameters for the TMP of Ti-6Al-4V during steckel mill rolling. However, analysis of the microstructural evolution across all three temperatures showed that three passes carried out at 950°C, 10/s, with interpass times of 44s and 77s, were the optimum parameters. Thus, steckel mill rolling of Ti-6Al-4V has been confirmed as a feasible process for the production of Ti-6Al-4V sheet material.

SYMBOLS AND ABBREVIATIONS

T_β Beta transus temperature

β Beta

α Alpha

α_p Primary alpha

TEM Transmission electron microscopy

EBSD Electron backscatter difrraction

α_{gb} Grain boundary alpha

α_w Widmanstätten alpha

α_{bw} Basket weave alpha

DRX Dynamic recrystallization

DRV Dynamic recovery

SIT Strain induced transformation

EDS Energy dispersive X-ray spectroscopy

ε Strain

ε_c Critical Strain

σ_c Critical stress

$\dot{\varepsilon}$ Strain rate

Z Zener-Hollomon parameter

Table of Contents

LIST OF FIGURES

LIST OF TABLES

LIST OF EQUATIONS

1. INTRODUCTION

1.1 Subject of Thesis

The subject of this thesis is to investigate the feasibility of using a steckel mill hot rolling schedule on the Ti-6Al-4V alloy. The influence of strain rate, temperature and interpass time on the microstructural evolution of Ti-6Al-4V will be assessed and statistical techniques employed to determine the optimum parameters suitable for the multi-pass thermo-mechanical processing (TMP) of Ti-6Al-4V.

1.2 Background to Thesis

Titanium and its alloys are renowned for their high specific strength, high formability and excellent corrosion resistance. As a result, they are widely used in the aerospace, biomedical and petrochemical industries. The Ti-6Al-4V alloy in particular has garnered the most attention, accounting for approximately 50% of titanium production worldwide. However, titanium is very expensive to produce, both in its extraction and subsequent processing. As a result, the use of titanium is limited to high performance industries, such as that of aerospace.

Although the extraction and refinement of titanium from its ore is expensive, it is not the single cause of titanium's high cost. Rather, it is the combination of refinement, ingot conversion and sheet-forming that makes this material and its alloys costly. This is shown in **Table 1**, where it can be observed that the fabrication of titanium into sheet material is 18 times more expensive than that of metals such as steel and aluminum. It can also be observed from this table that the secondary processing or sheet-forming of titanium is costlier than ingot production or the refinement of the metal. In addition, the slow speeds used during forging and other secondary fabrication methods further serve to make TMP of titanium a time-consuming and laborious affair. Lastly, the loss of material during sheet-forming from an ingot results in low yields. It is for this reason that faster, cost-effective methods of producing Ti-6Al-4V sheet are being

investigated. Should such methods be identified and implemented, titanium and its alloys will be cheaper and more accessible. One of the methods under consideration for the sheet forming of Ti-6Al-4V is steckel mill rolling.

Table 1. A breakdown of thermo-mechanical processing of titanium in comparison to steel and aluminum[1].

Production Stage	Steel	Aluminum	Titanium
Metal refining	0.4	1.0	5.0
Ingot forming	0.6	1.0	10.7
Sheet forming	0.4	1.0	18.0

A steckel mill is a two-stand reversing mill with two coiler furnaces on either side. The purpose of these furnaces is to anneal the metal strip between passes, thereby ensuring that a metal strip is maintained at high temperature throughout processing. Because of this, passes can be completed in a short period time (approximately six minutes compared to more than 25 hours for titanium)until a desired gauge thickness is achieved[1,2]. Traditionally, a steckel mill is used for the manufacture of steel sheet although it may be used for sheet production of other materials, such as brass. The main advantage of a steckel mill is its low capital cost, which makes the production of steel sheet an inexpensive process. A steckel mill is also capable of producing 1.5 million tons of stainless steel products annually. Therefore, steckel mill rolling represents a faster, cost-saving alternative for the production of Ti-6Al-4V sheet.

1.3 Objectives of Thesis

The aims of this research were:

i. To investigate the feasibility of using on Ti-6Al-4V a multi-pass deformation schedule similar to that employed in a steckel mill for the hot rolling of stainless steel.

ii. To assess and characterise the microstructural evolution that arises when Ti-6Al-4V undergoes multi-pass hot deformation.

iii. To use statistical analysis to ascertain the optimum processing parameters of temperature, strain and interpass time, suitable for the thermomechanical processing of Ti-6Al-4V in a steckel mill.

2. LITERATURE REVIEW

2.1 Introduction to Titanium

Titanium has excellent properties, such as a high strength-to-weight ratio, high corrosion resistance and high strength at high temperatures. **Figure 1** shows the specific strength vs. temperature of titanium and its alloys compared to other materials. From this Figure, it can be seen that titanium and its alloys have a higher specific strength than those of steel and superalloys. It can also be observed that, although carbon fiber reinforced polymer (CFRP) has a greater specific strength than titanium, its use is limited to temperatures of not more than 600°C, whereas titanium alloys can be used at temperatures exceeding 750°C. Because of its bio-compatibility, titanium is often used in joint replacement surgeries, as well as in cranium replacement, where its low density is also exploited. Moreover, titanium and its alloys are able to form a thin film of oxide when exposed to highly corrosive environments and thus display a corrosive resistance that surpasses even that of stainless steels. It is for this reason that titanium and its alloys are employed in highly corrosive environments, such as those in the petrochemical industry[3]. However, despite all its attractive properties, titanium and its alloys are still more expensive to process and fabricate than stainless steel and aluminum. As a result, the use of this metal is mainly limited to aerospace applications[4].

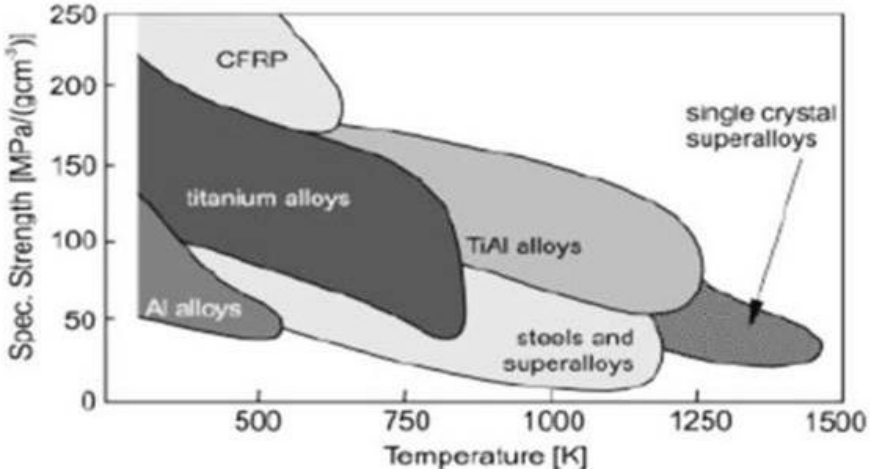

Figure 1. The specific strength of Ti and its alloys at high temperatures in comparison to other metals[5].

Titanium (Ti) is an allotropic metal, that is, depending on the temperature it is subjected to, it exists as either the alpha (α) phase or the beta (β) phase. The crystal structures of the α and β phases are hexagonal close-packed (HCP) and body-centered cubic (BCC), respectively. In HCP Ti-6Al-4V, there are three slip directions and these are given by $< 11\bar{2}0 >$ and one slip plane - the basal plane- given by (0002).This gives rise to three slip systems (*slip system=system plane x slip direction)*.The addition of alloying elements to Ti-6Al-4V leads to the $(10\bar{1}0)$ prismatic planes being favoured over the basal plane as this increases their packing density. This then results in four independent slip systems. In contrast, the BCC crystal structure has 12 slip systems: two $\langle 111 \rangle$ slip directions and six $\{110\}$ slip planes. The increased number of slip systems in the BCC crystal structure is the reason the beta phase is easier to plastically deform than the alpha phase[4]. In **Figure 2**, the unit cells of the α and β phase are shown.

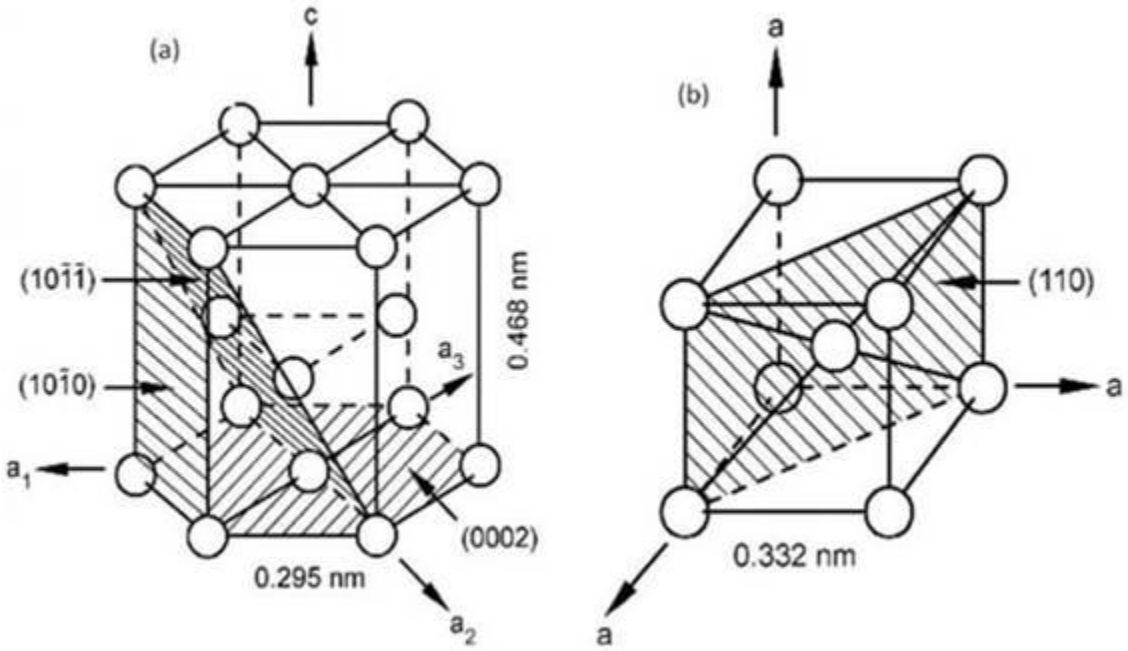

Figure 2. The unit cells of (a) the α phase and (b) the β phase[4,6].

The temperature at which pure titanium undergoes an allotropic transformation from the α to the β phase is termed the beta transus (T_β) temperature. The T_β in pure Ti is 882.5°C, but it can be affected by alloying elements, which can stabilise either the α phase by raising the β transus or the β phase, thereby lowering the beta transus temperature[4].

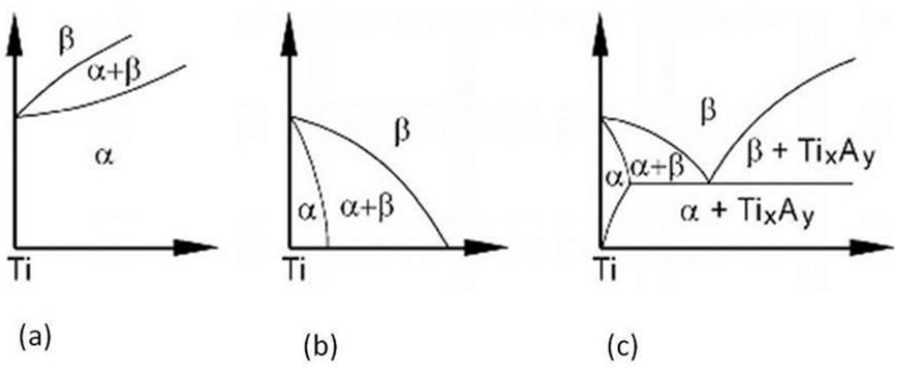

Figure 3. The effect of (a) α, (b) β isomorphous and (c) eutectoid forming stabilisers on the T_β of titanium (Adapted from Lutjering and Williams)[4].

α Stabilisers

Certain alloying elements, such as aluminium (Al), and interstitial atoms, such as oxygen (O), nitrogen (N) and carbon (C), stabilise the α phase by increasing the T_β as the alloying element content increases. **Figure 3** (a) demonstrates the effect of α stabilisers in alloyed titanium.

β Stabilisers

These stabilise the β phase up to room temperature. The alloying elements vanadium (V), molybdenum (Mo) and niobium (Nb) are commonly-used β phase stabilisers, known as β isomorphous elements. β isomorphous elements yield the phase diagram shown in **Figure 3** (b) [1]. Another class of β stabilising alloying elements is known as eutectoid forming. Alloying elements in this class are chromium (Cr), iron (Fe), silicon (Si) and hydrogen (H). The phase diagram shown in **Figure 3** (c) is typical of β eutectoid-forming elements.

α-β Alloys

The addition of sufficient concentrations of α and β stabilising elements leads to the existence of both α and β phases simultaneously at room temperature. Such alloys are known as alpha-beta (α+β) alloys, of which Ti-6Al-4V is an example. The phase diagram of α+β alloys is given in **Figure 3** (b).

2.2 Phase Transformations in Ti-6Al-4V

The beta transus temperature of Ti-6Al-4V is quoted as 995±20°C[7]. When heated from room temperature to high temperatures within the α + β region, as well as above the T_β, Ti-6Al-4V undergoes a diffusional (α to β) phase transformation. From **Figure 4** it can be observed that once high temperatures within the α+β region have been reached, the volume fraction of the β phase increases rapidly, and more so at temperatures above 800°C[6].

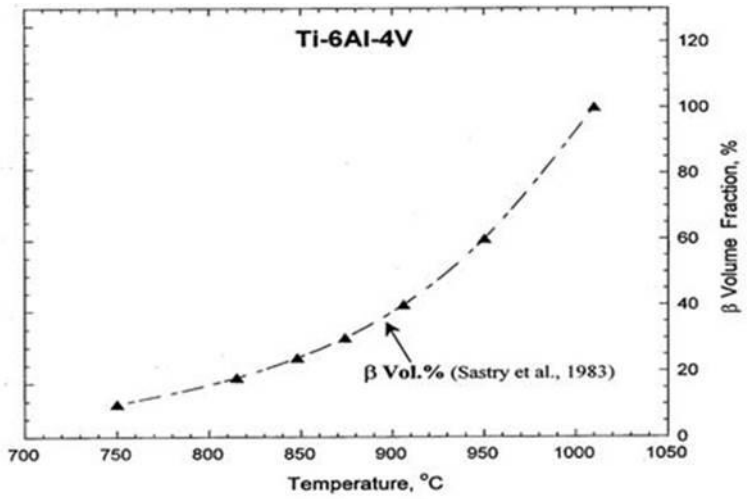

Figure 4. The volume fraction of the β phase vs. temperature (adapted from Sesacharyulu*etal.*)[6].

However, on cooling, Ti-Al-4Vphase transformations in Ti-6Al-4V can either be diffusionless or diffusion controlled. The type of transformation that occurs is dependent on the cooling rate that the alloy is subjected to when cooled from above the T_β[4,8].

2.2.1 Crystallographic Relationship between the α and β Phases

The crystallographic relationship between the β and α phases is such that $(110)_\beta \parallel (0001)_\alpha$ and $[\bar{1}11]_\beta \parallel [11\bar{2}0]_\alpha$. This is known as the Burgers Orientation Relationship. According to this relationship, an HCP crystal can have 12 hexagonal variants, with each variant having a different orientation to the parent β crystal. Consequently, the α phase assumes a needle, lath, lamellar or

plate morphology. The Burgers Orientation Relationship has been found to be obeyed by both diffusionless and diffusion controlled phase transformations[4].

2.2.2 Diffusion Controlled Phase Transformations

When Ti-6Al-4V is cooled from above, the T_β at rates below 20°C/s, grain boundary α (α_{gb}), begins to nucleate and grow at prior β grain boundaries. This type of α phase is restricted to the β grain boundaries and is termed an alliomotroph[8]. Growth of α_{gb} proceeds continuously or discontinuously until the entire β grain boundary is covered by this phase [**Figure 5** (b)]. As cooling progresses, parallel plates of the α phase begin to grow into the prior β grain, forming colonies of Widmanstätten α (α_w), with each plate delineated by the β phase [**Figure 5** (d)].These colonies eventually join up with colonies that formed from other points within the same prior β grain. Once the formation of colony Widmanstätten is complete, the last variant of α_w forms in a pseudo random fashion within the parent β grain. This type of α_w is known as basket weave α. The formation of basket weave α is not only cooling rate dependent, but also affected by beta stabiliser composition. At high cooling rates, but not so high as to have a diffusionless phase transformation take place, the growth of α plates is restricted, so the formation of basket weave α is favoured. Also, as β stabiliser content increases, the formation of basket weave α will be more likely than colony α_w for a given cooling rate. This is due to high beta stabiliser concentrations' requiring less undercooling[8–10].

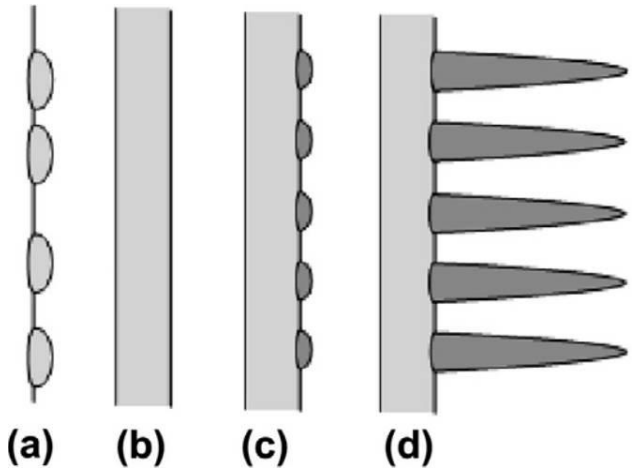

Figure 5. Schematic depicting the formation of Widmanstätten α in Ti-6Al-4V[11].

2.2.3 Diffusionless Phase Transformation

Diffusionless phase transformations in β isomorphous alloys results in the formation of martensite. The martensite can either be (α') or (α"). α' can be further classed into acicular and massive martensite. According to Lutjering and Williams, α' acicular martensite is common in alloys with a high solute content and a low martensite transformation temperature[4]. However, massive martensite is associated with pure Ti, dilute alloys and alloys with a high martensitic transformation temperature. It has also been observed in some Ti-X eutectoid systems[12]. X in these eutectoid systems can either be Si, Au or Ag. α" martensite is a supersaturated orthorhombic phase, observed in alloys with a high β stabiliser content, and is thus rarely seen in Ti-6Al-4V[7].

2.2.4 Acicular and Massive α Martensite

Acicular or plate martensite comes about as a result of quenching Ti6Al4V from above the beta transus temperature at cooling rates in excess of 410°C/s[8,12,13]. During this transformation, a cooperative movement of atoms occurs, resulting in the transformation from the BCC crystal lattice of the β phase to the HCP crystal lattice of the α' phase[4,7,8].The microstructure of acicular martensite consists of individual plates that have a 30°, 60° and 90° orientation to one another.

Furthermore, the substructure of acicular martensite consists of stacking faults, dislocations and twins. It should be noted that owing to the diffusionless nature of this transformation, this phase is compositionally invariant, that is, it has the same composition as the β phase. The concentration of solute or β-stabiliser also influences the formation of plate martensite. As such, when the alloy is quenched from high temperatures with the α+β phase region, at a temperature above the martensite start (M_S) temperature and a quench rate greater than 410°C/s, acicular martensite may form and some beta phase retained[8]. The microstructure of acicular martensite is shown in **Figure 6**.

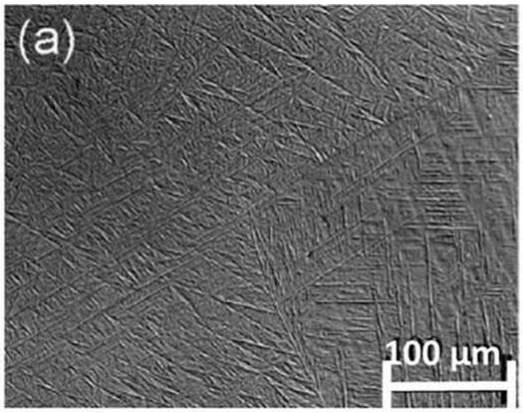

Figure 6. Acicular martensite in Ti-6Al-4V[14]

At moderate quench rates between 20°C/s and 410°C/s, Ti6Al4V forms massive α martensite when quenched from above the T_β. The transformation of the β phase to massive martensite is competitive with both martensitic and diffusion controlled transformations, so it is essential that the cooling rate be sufficiently low to allow for the formation of massive α. While the massive transformation is trans-interfacial (short range), it, like acicular martensite, has an HCP crystal structure and is compositionally invariant. Massive α martensite is often referred to as packet or lath martensite owing to the presence of large, irregular regions that contain small parallel plates about 0.5-1µm in size within its microstructure[7]. Retention of the β phase is not observed in packet martensite[13]. The micrograph in **Figure 7** shows that massive α forms at prior β grain boundaries and at acicular martensite plates within the prior beta grain, as well as at individual acicular martensite plates. The influence of the cooling rate is such that the occurrence of massive α increases with the decrease of cooling rate.

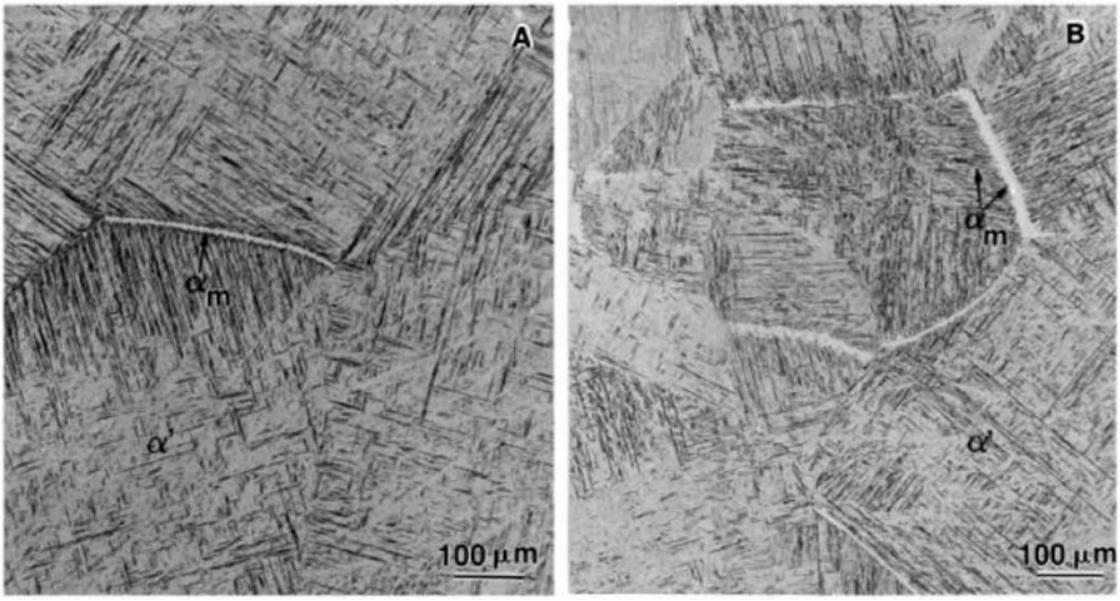

Figure 7. Massive martensite in Ti-6Al-4V cooled at (a) 410°C/s, (b) 275°C/s[13].

2.2.5 Production of Ti alloys

Ingot Conversion

An ingot can be produced using either vacuum arc remelting (VAR), where an atmospheric pressure of 10^{-2} Pa is used[15], or cold hearth melting. During VAR, sponge obtained from the Kroll process and scrap known as revert are fed into an electric arc furnace and melted. After the first melt, the surface of the ingot is ground and contaminants removed. For the purposes of homogeneity and the dissolution of oxygen- or nitrogen-related defects, the ingot is melted for a second time[1,16]. If the application that the alloy is to be used for is one where quality is critical, the ingot must be remelted a third time. The main disadvantage of VAR is that it can result in high density inclusions (HDIs). These occur when the electrode used to melt the input material comes into contact with elements, such as tungsten carbide (WC) attached to the revert that was used in welds. Since these inclusions have a high melting point they are, as a result, difficult to expel. It is for this reason that VAR requires a large labour force, as the process requires that

great care be taken in preparing the electrode and, because of the multiple melts, it is also time-consuming[1].

A more recent method used in ingot production is cold hearth melting and, depending on the source of heat, it can be termed plasma arc melting (PAM) or electron beam melting (EBM)[7]. The process of melting is similar to that employed in VAR, except that the copper crucible bears a solid titanium "skull", over which molten titanium runs. As the molten titanium is always in contact with this skull, contamination from the hearth does not occur. Unlike in VAR, where everything from the electrode becomes part of the final ingot, in cold hearth melting the HDIs, being of a higher density than titanium, sink and are embedded in the skull[1]. Another advantage of cold hearth melting is that the loss of material is limited, as slabs and bars, which are more suitable for conversion into sheet form, can be cast, using cold copper hearth melting[5]. However, there is a downside to cold hearth melting, in that it cannot be used as a stand-alone method, but must, for the purposes of rotor grade material, be used in conjunction with VAR. For this reason, copper hearth products are slightly more expensive than vacuum arc remelted ingots.

2.2.6 Industrial Thermo-mechanical processing of Ti-6Al-4V

In industry, the thermo-mechanical processing of Ti-6Al-4V consists of ingot breakdown or primary fabrication and secondary fabrication.

Primary Fabrication

This is the also known as ingot breakdown and involves the use of techniques such as hot rolling or forging. The purpose of these is to break down the microstructure from casting, consisting of coarse lamellar colonies approximately 200-500 μm in size. This is done by β forging at temperatures 100 - 150°C above the T_β. Recrystallisation at temperatures 50 - 75 °C above the T_β is then carried out and the result is microstructure consisting of finer lamellar colonies[16]. The schematic for this process can be seen in **Figure 8**. Once cooled, the alloy is aged for stress relief and strengthening.

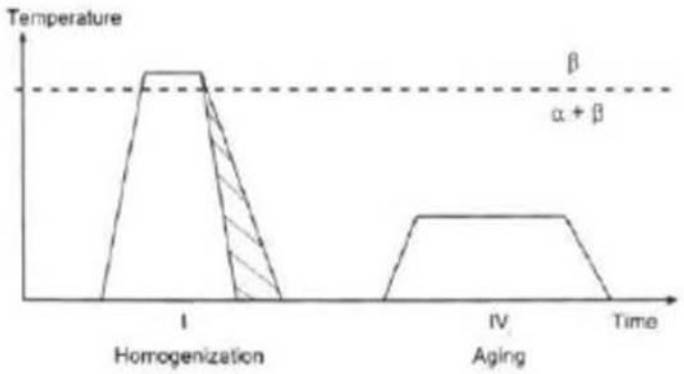

Figure 8. Schematic used to generate a lamellar microstructure in Ti-6Al-4V[4].

The challenges that arise during primary fabrication are due mainly to titanium being prone to oxidation. Consequently, the surface of the bar or slab must be ground constantly, resulting in loss of material[17].

Secondary Fabrication

This is the stage where components are fashioned. Methods used here include forging, extrusion, hot forming and machining. The choice of method used is dependent on the final product required. After secondary fabrication, the resultant microstructure can either be bimodal or equiaxed.

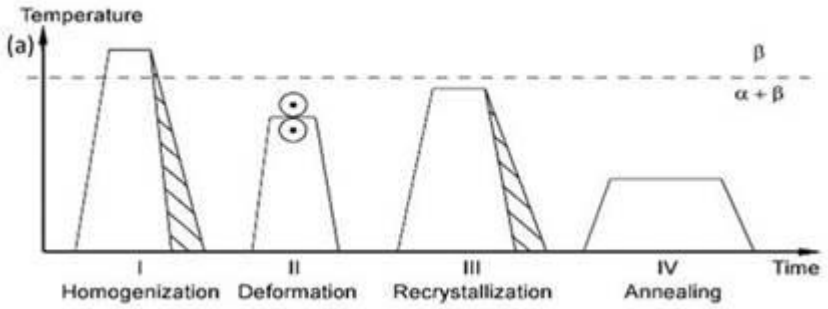

Figure 9. Schematic showing the deformation schedule used to produce a bi-modal or equiaxed microstructure[4].

Bimodal microstructure

The formation of a bimodal microstructure in Ti-6Al-4V requires that the lamellae obtained after the homogenisation step in **Figure 10** (a) be plastically deformed. This deformation takes place in the α+β phase field and should be as high as possible so as to increase the stored energy, which will be the driving force for recrystallisation. During recrystallisation, the deformed lamellae are transformed into equiaxed primary α (α_p), through a mechanism known as globularisation[6]. The cooling rate after step III is also important, as a fast cooling rate results in coarser equiaxed α_p and coarser α+β lamellae, while a slower cooling rate results in finer lamellae and finer equiaxed α_p[5] [**Figure 10** (b)].

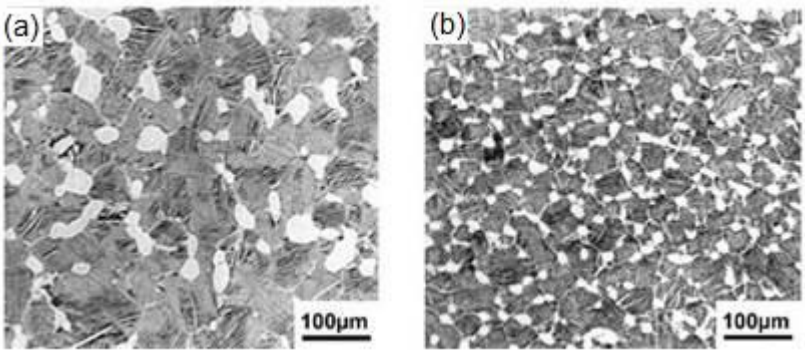

Figure 10.(a) Bimodal microstructure obtained after slow cooling, (b) bimodal microstructure obtained after fast cooling[4].

Equiaxed Microstructure

A fully equiaxed microstructure is also acquired according to the processing schedule shown in Figure 9. However, in this case, the recrystallisation (step III) is done at very low temperatures within the α+β phase region. This is so that the formation of a fully lamellar microstructure is suppressed. Instead, the β phase forms at the triple junctions of α grains. The α grain size in this case will be larger than the α_p observed in a bimodal microstructure[5,7], as presented in **Figure 11** (a).

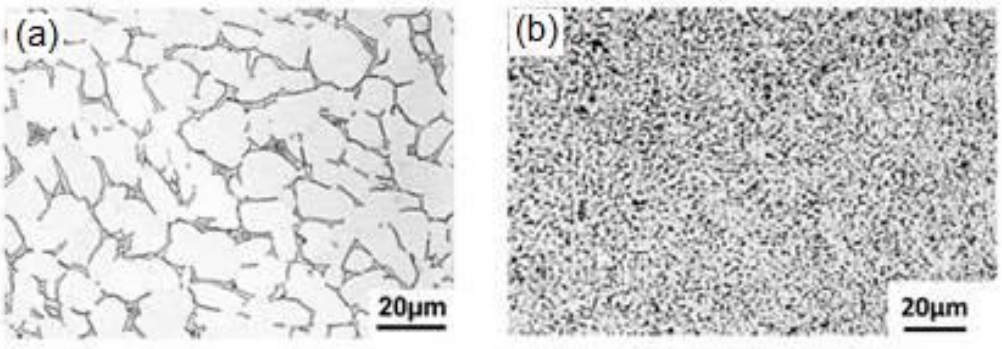

Figure 11. (a)equiaxed microstructure produced after (a) slow cooling and (b) equiaxed microstructure produced after fast cooling[4].

2.3 The Deformed State

2.3.1 Stored Energy

During plastic deformation, dislocations, vacancies and point defects are created within the material. Moreover, these dislocations increase and their motion is inhibited as deformation proceeds. A higher stress must then be applied to again set the dislocations in motion and this causes work hardening. The result is an increase of energy within the material, of which 99% is given off as heat and the rest stored[18]. The stored energy is mainly from dislocations, as the point defects and vacancies do not contribute significantly. It is the release of this energy that serves as the driving force towards restoration mechanisms such as recovery and recrystallisation. An increase in either strain rate or strain increases the number of dislocations within the material and thus is the driving force for recrystallisation or recovery. The stored energy can also be increased by performing deformation at lower temperatures. Therefore, it can be rationalised that the driving force for recrystallisation will be higher when deformation is carried out at low temperatures using high strains and strain rates.

2.3.2 Stacking Fault Energy

The mode of deformation during thermomechanical processing is determined by the metal's stacking fault energy (γ SFE). In metals with a high γ SFE, the preferred mode of deformation is through slip or climb. Furthermore, metals such as these undergo recovery as a restoration mechanism. The lack of slip systems in metals with a low γSFE results in their undergoing twinning as a deformation mode and dynamic recrystallisation, although recovery may occur to a certain extent[19]. In Ti-6Al-4V, the beta phase has a high SFE and deforms by slip. It has been established that the restoration mechanism that this phase undergoes on deformation at temperatures above the beta transus is recrystallisation[18,20]. At temperatures below the beta transus, where both the α and β phase exist, twinning as a deformation mode is inhibited owing to the presence of alloying elements.

Once a metal has been deformed, its mechanical properties can be restored through annealing it at high temperatures for a certain period of time. Although dislocations are arranged into lower energy configurations during annealing, grain boundaries remain unaffected. Subsequent annihilation and rearrangement of these dislocations lead to their forming subgrains. This is known as recovery.

For recovery to occur a metal needs to be cold-worked and subsequently annealed but the process can also occur during deformation of the metal at high temperatures. In this instance, it is known as dynamic recovery (DRV). If dynamic recovery has occurred, the stress-strain curve typically resembles the one observed in **Figure 12** (b). However, as the strain rate is increased during deformation, adiabatic heating may occur, resulting in the reduction of flow stress. Consequently, the stress-strain curve will exhibit flow softening. Post-deformation annealing following DRV does not result in further recovery, but rather the coarsening of subgrains[20].

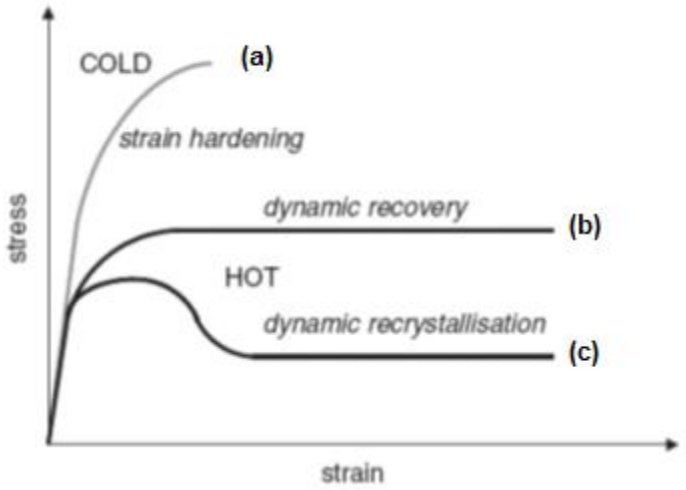

Figure 12. Stress-Strain curves showing features of cold and hot deformation[18].

2.3.3 Recrystallisation

During this process, new grains, free from dislocations, nucleate at high angle grain boundaries (misorientation angle > 15°) and at dislocations within the deformed or recovered microstructure. These then grow and consume old grains, resulting in a microstructure consisting of new grains. When recrystallisation occurs, high angle grain boundaries migrate through the transfer of atoms to and from the grains that are adjacent to the boundary. Where recrystallisation occurs during deformation at high temperatures, it is termed dynamic recrystallisation (DRX). For DRX to occur, a critical strain (ε_c) must be reached and this is before the peak of the stress-strain curve, as observed in **Figure 13** (c). This value increases with a decrease in deformation temperature and a decrease in strain rate[18,20].

Recrystallisation initiates at old grain boundaries through the nucleation and subsequent growth of new grains. The process is repeated until the microstructure consists solely of fully recrystallised grains [**Figure 13** (a)-(e)]. During the recrystallisation process grain growth does not occur, because the dislocation density of new grains increases as deformation proceeds. Moreover, the continued migration of high angle grain boundaries further serves to inhibit grain growth. However, if a high temperature is maintained and deformation is terminated, static recrystallisation and grain growth will ensue, as the new grains will not incur further dislocations[3,21].

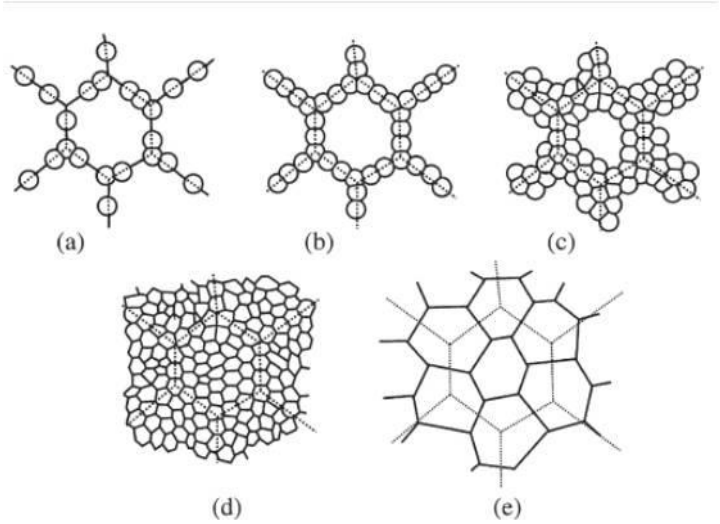

Figure 13. Resultant recrystallised grain size if the initial grain size is (a-d) large and (e) small[18].

Where DRX has occurred, flow stress curves exhibit a broad peak, followed by a decrease in flow stress into a plateau, as shown in **Figure 13** (c). It has been postulated that a small initial grain size (D_0) results in a single broad peak in the stress-strain curve[18]. If D_0 is small, the material is always partially recrystallised owing to lack of sites for recrystallisation. Consequently, because new grains are always continuously forming while deformation proceeds, the flow stress curve is averaged out into a single peak. However, if the starting grain size (D_0) is large, then there are enough sites for recrystallisation to complete before another cycle of recrystallisation begins[20]. This leads to the oscillatory flow curve observed in **Figure 14**. Another reason that has been given for oscillatory flow stress is that, at low strain rates, a cycle of recrystallisation is initiated and completed before another one begins. The result is a true stress-true strain curve, showing cyclical behaviour. However, at higher strain rates, the flow stress shows a single broad peak that eventually decreases into a plateau. This is expected for deformation at a high strain rate, because parts of the microstructure have recrystallised and, before this is complete, another cycle of Rx has begun, and so forth. The result is a sum of all these incomplete recrystallisation cycles, which is a broad peak[18].

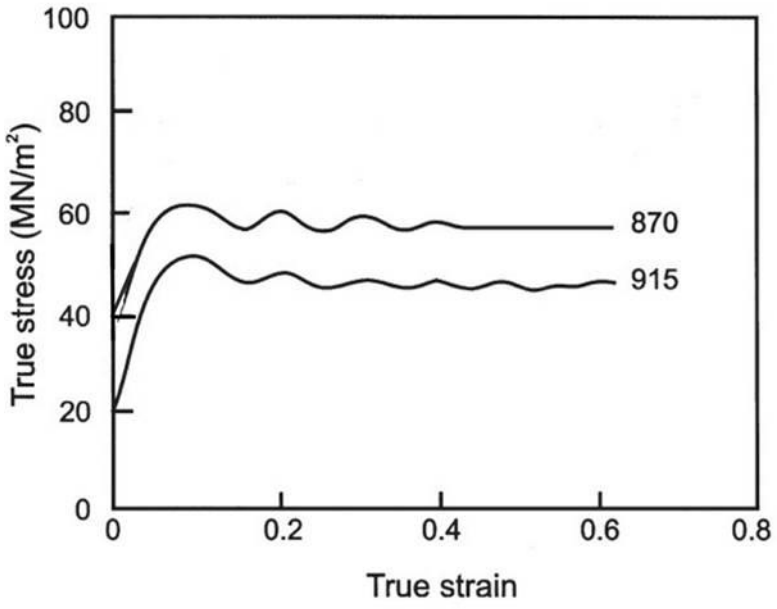

Figure 14. Oscillatory true stress-true strain curves, showing the dynamic recrystallisation of 0.68% C steel (adapted from F. J. Humphreys)[18].

2.3.4 The Zener-Hollomon Parameter (Z)

The relationship between strain rate and temperature during hot deformation is expressed by:

$$Z = \dot{\varepsilon} e^{\frac{Q}{RT}}$$ **Equation 1**

where: $\dot{\varepsilon}$ is the strain rate, Q is the activation energy (J/mol), R is the gas constant and T is the temperature.

This relationship is useful in deducing whether a metal will undergo flow softening or strain hardening during deformation. A high Z-value indicates that the metal will work harden, while a low value of Z means that the material will soften. Under conditions of high Z, it must be considered that adiabatic heating may occur during strain hardening, with flow softening the consequence. The features observed in **Figure 12** (b) and (c), as well as in **Figure 14** can be elucidated using the Z parameter.

2.3.5 Grain Growth

Once recrystallisation has occurred and a high temperature is maintained, the growth of recrystallised grains occurs rapidly[18]. While the microstructure is now free of dislocations following recrystallisation, the grain boundaries are thermodynamically unstable. As such, the grain boundary area must be reduced and this can be achieved either through larger grains growing and consuming smaller grains so that the grain size distribution is consistent (normal grain growth) or by certain favourably oriented grains growing in preference to others (abnormal grain growth)[2]. This is illustrated in **Figure 15**.

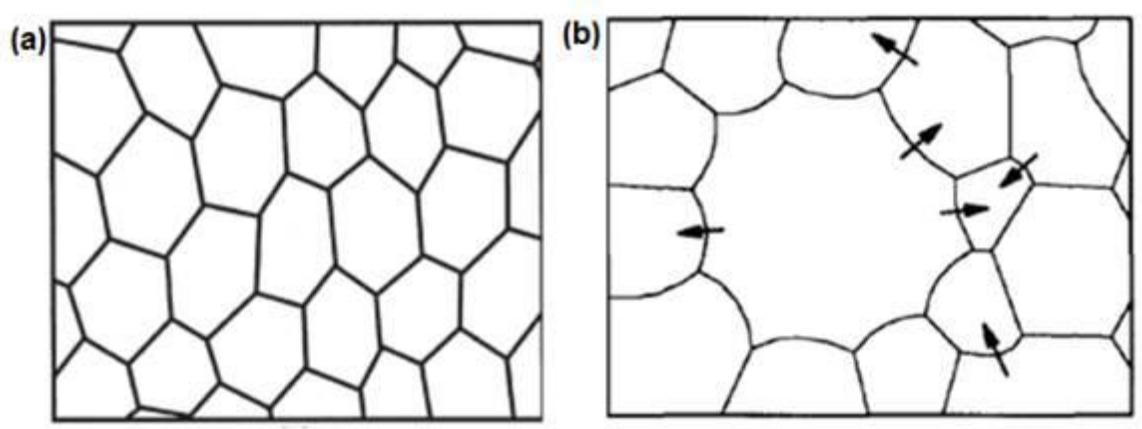

Figure 15. (a) normal and (b) abnormal grain growth following recrystallisation[18].

2.3.6 Influence of Processing Parameters on the TMP of Ti-6Al-4V

The mechanical properties of Ti-6Al-4V following deformation are dependent on processing parameters such as the strain, strain rate and temperature[6,17,18,22].Figure 16 shows the true stress-true strain curves of Ti-6Al-4V with an equiaxed preform. From this figure it can be observed that the influence of strain rate is such that the flow stress increases with an increase in strain rate for a given temperature and that an increase in temperature results in a significant decrease in flow stress, regardless of strain rate. This trend has been found to be true for Ti-6Al-4V, regardless of the preform microstructure[3,23]. A closer study of **Figure 16** further reveals that at strain rates $\leq$ 1/s, the material displays steady state behaviour irrespective of whether the temperature is above or below the T_β.

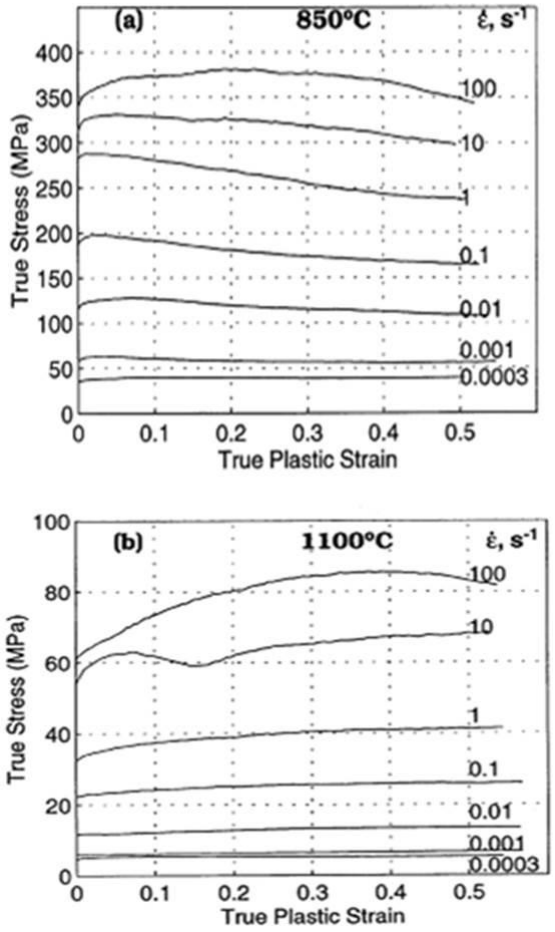

Figure 16. True stress-true strain curves, showing the influence of strain and temperature on the flow stress of Ti-6Al-4V when deformed at (a) 850°C and (b)1100°C[6].

Steady state behaviour in the flow stress is a result of work hardening and softening mechanisms occurring at the same rate. It is attributed to dynamic recovery at temperatures within the α+β phase region and deemed to be a consequence of dynamic recrystallisation of β grains at temperatures above the T_β[6,19].This is shown in **Figure 17** below.

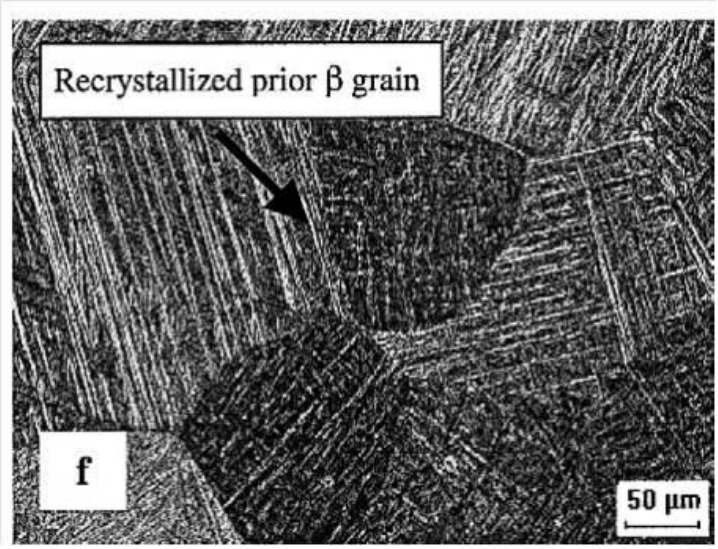

Figure 17. Recrystallised β grains of a Ti-6Al-4V sample deformed at 1050°C, 0.5/s[24].

At strain rates above 1/s, flow softening is observed at both the two-phase and single-phase regions [**Figure 16**]. This phenomenon has been explained to be brought about by adiabatic heating at temperatures below transus and by flow instability at temperatures above the T_β[6].

2.3.7 Processing Maps

In industry, processing maps are used to establish process parameters where a metal can be hot rolled, extruded or hot forged without bringing about defects. Processing maps are generated using hot compression data, acquired over extensive temperature and strain rate ranges and the various microstructural mechanisms that occur under various temperature and strain rate conditions are identified[25]. **Figure 18** below shows a processing map for Ti-6Al-4V with an equiaxed preform microstructure at a temperature range between 750°C and 1100°C and a strain rate range of 3×10^{-4} to 100/s. It can be seen from this figure that, in order to avoid the formation of adiabatic shear bands during thermomechanical processing below the T_β, hot deformation should be done at strain rates below 1/s. Instability above the beta transus, as well at sub transus temperatures, can be circumvented through hot working the alloy at strain rates below 10/s[6,25,26].

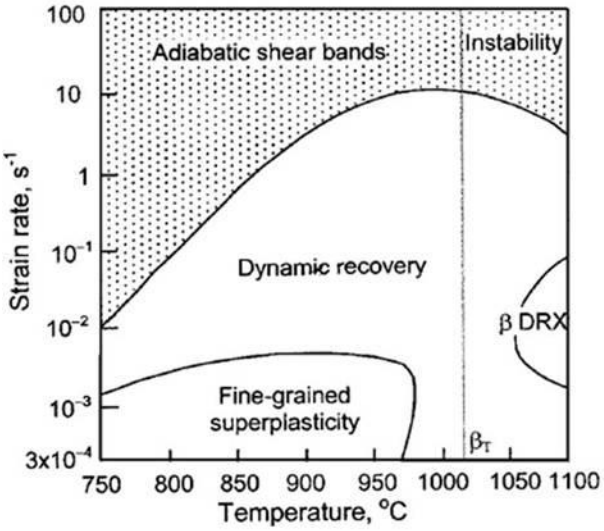

Figure 18. Processing map for Ti-6Al-4V with an equiaxed microstructure[25].

2.3.8 Microstructural Defects

The hot deformation of Ti-6Al-4V, using parameters exceeding those stipulated in processing maps, results in the formation of microstructural defects. These include shear bands, as well as flow instability, within the microstructure.

Adiabatic Heating and Adiabatic Shear bands

Titanium and its alloys possess low heat conductivity and are thus unable to dissipate heat during deformation. This leads to an increase in the temperature of the specimen. As the temperature of Ti-6Al-4V increases, so too does the volume fraction of the β phase and this further contributes towards the softening of the alloy. At high strain rates the inability to disperse heat is exacerbated and may result in the formation of shear bands. Adiabatic shear bands are regions of highly localised deformation that arise as a consequence of deformation at high strain rates. Adiabatic shear bands are considered defects as their formation results in the flow softening of a material and its subsequent failure. In Ti-6Al-4V, deformation temperatures of approximately 750°C and strain rates of 10^{-2} result in the failure of the material through the formation of adiabatic shear bands during hot compression[27]. A micrograph, as well as a macrograph showing Ti-6Al-4V that has failed through the formation of shear bands, can be seen in **Figure 19**.

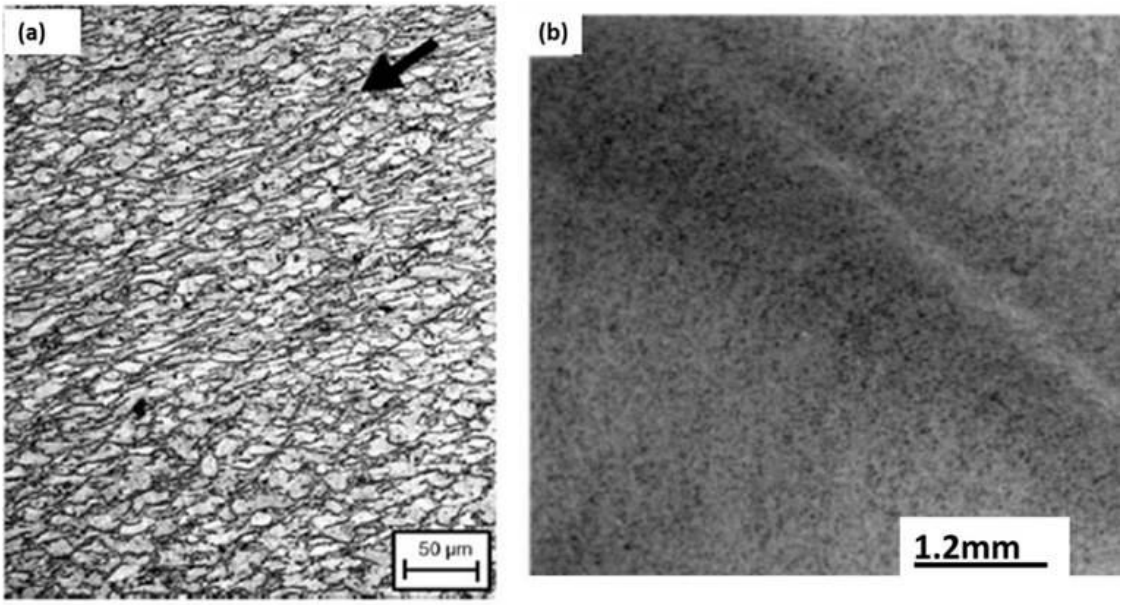

Figure 19. (a) A micrograph and (b) a macrograph, showing shear bands in a Ti-6Al-4V sample deformed at 850, 10/s[19].

At temperatures above the beta transus and strain rates above 10/s, deformation results in flow instability within the microstructure. However, owing to the phase transformation that occurs on cooling Ti-6Al-4V from above the T_β, the microstructural features of flow instability at this temperature cannot be acquired[19]. Instead, flow instability at this temperature manifests as flow oscillations in the stress-strain curve, as shown in **Figure 14**.

2.3.9 Globularisation

Globularisation is a process whereby α lamellae in titanium and its alloys are transformed into α globules during deformation below the T_β. Globularisation may also arise during heat treatment of the metal after hot working. In both instances, globularisation results in flow softening and it is believed to occur in two ways:

2.3.10 Boundary splitting

This is where lamellae are fragmented owing to intense localised shear within α α lamellae/plates during deformation and subsequent annealing below the T_β. The driving force for boundary splitting is the instability of 90° dihedral angles between interphase α/β boundaries and interphase α/α boundaries[27]. This then leads to surface tension penetration of α platelets by the β phase[27]. In a study by Zhebtstrov*et al.*[28], as well as one by Margolin and Chen[29], it was found that large strains ($\varepsilon > 1.2$) must be imparted on the metal in order to achieve a fully globularised microstructure through this mechanism. However, Semiatin *et al.*[27]argue that strains between 0.75 and 2 are required to initiate and see globularisation to completion.

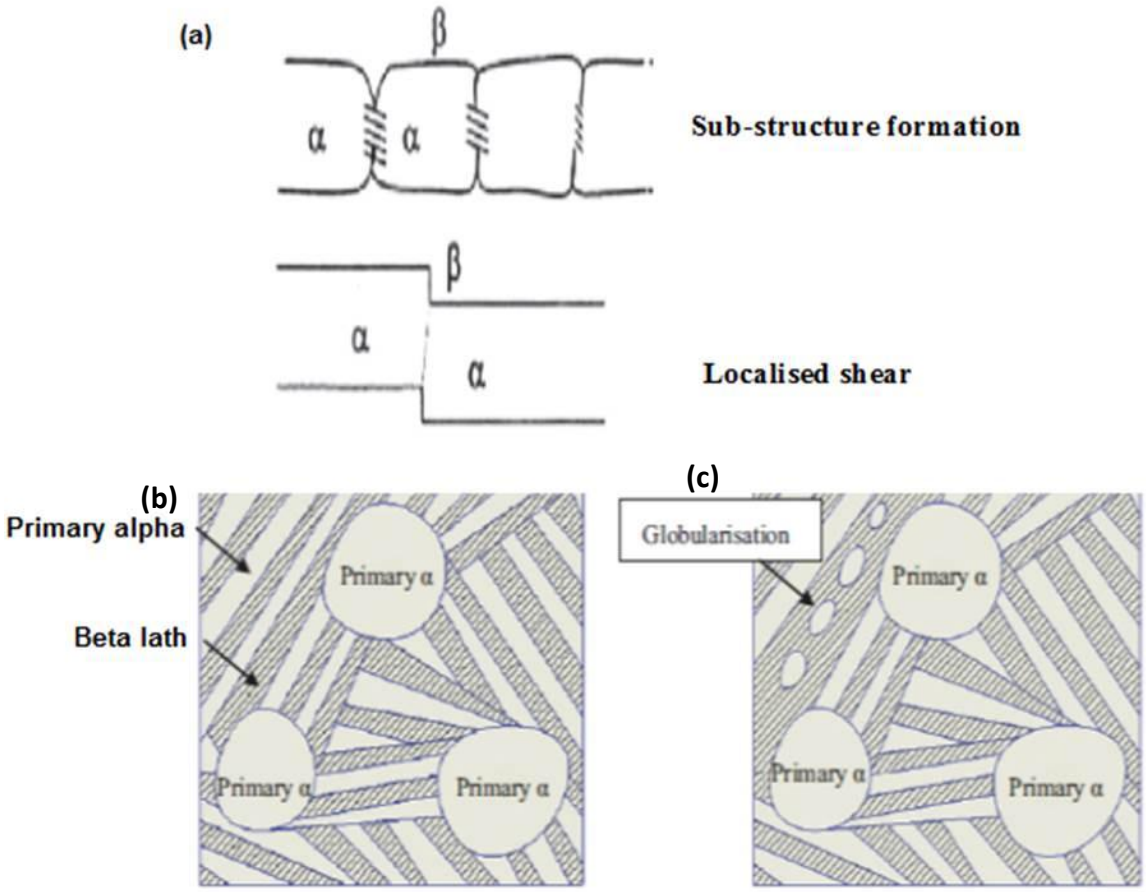

Figure 20. The process of globularisation of an α plate in titanium shown to occur by (a) formation of substructures in the α plate, leading to subsequent localised shear, and (b), a schematic of globularisation in Ti-6Al-4V with a bi-modal microstructure[28].

2.3.11 Termination Migration

The diffusional coarsening and spherodisation of lamellar platelets during heat treatment of titanium is known as termination migration. The difference in solute concentration between the curved edge of one platelet and the flat surface of a neighbouring platelet is the cause of this diffusion. As diffusion occurs, the edges of the plates shrink back, while those towards which diffusion is happening, coarsen. In α/β alloys this is dependent on the energy associated with interphase boundaries and it can be raised by deforming the material at high temperatures[27,30].

2.4 Mechanical properties

In Ti-6Al-4V, the influence of microstructure is such that a fully lamellar microstructure has superior creep resistance and better fatigue properties when compared to bimodal and equiaxed microstructures. However, cracks propagate much faster in lamellar microstructures owing to the lamellae providing longer paths for a crack to advance[31]. It is for this reason, in addition to the lack of ductility at room temperature by this microstructure, that equiaxed and bi-modal microstructures are preferred. In **Figure 21**, it can be seen that the strength increases in the order of equiaxed, lamellar and bimodal microstructures. It can also be observed that the equiaxed microstructure displays a combination of ductility and strength, which is why it is preferred as the final microstructure of titanium components[6].

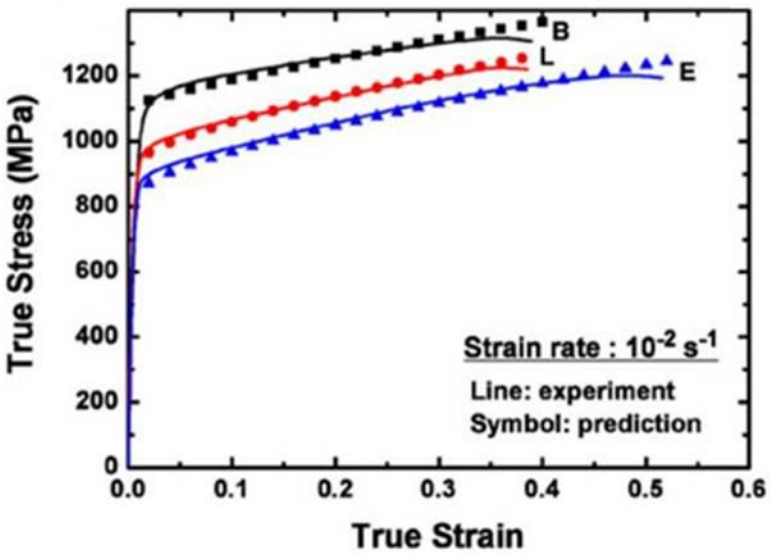

Figure 21. A comparison of the mechanical properties of the equiaxed, lamellar and bimodal microstructures[32].

2.5 The Steckel Mill

A steckel mill is a two-stand reversing mill that consists of work and back up rolls. Invented in the 1930s, the steckel mill has been traditionally used for the production of steel sheet or plate. It was only in 1980 that that the first single-stand steckel mill was constructed, in Middleburg, South Africa, and it could accommodate other materials, such as brass and super alloys[33]. In

comparison to a traditional hot strip mill, a steckel mill has two hot coiler furnaces on either side to replace the six stands found in a conventional mill, [**Figure 22** (b)]. During processing, the strip loses heat to the surroundings, and more so as the gauge becomes thinner, which then increases the rolling forces required to deform the strip. Thus, the function of these furnaces, whose temperature is set between 970°C and 1000°C, is to keep the temperature of the metal strip elevated throughout processing so that reversing passes can continue indefinitely[2].

Before steckel mill rolling can proceed, a transfer bar from a roughing mill is first cropped to a height of 25mm or 35mm. Once the bar is fed into the steckel mill it is referred to as a strip. The strip can be considered as having three parts: the head, which enters the mill first, the mid-section, and the tail, which enters the mill last. The head end of the strip is passed under the furnace on the entry side of the steckel mill and is threaded through the roll gap. It then passes through the work rolls and is fed into the furnace on the delivery side at the pinch roll unit [**Figure 22** (a)]. After a set period of time, the strip is released, again passed through the work rolls and fed into the furnace on the entry side, thereby completing the second pass. Passes can continue three, five, seven or nine times, until a gauge thickness of 2.5mm is achieved[33].

The parameters of importance during the steckel mill rolling process are the temperature (T), the strain rate ($\dot{\varepsilon}$), the strain (ε) and the interpass time (t). The interpass time is defined as the amount of time that the strip spends within the coiler furnaces between passes. This parameter is of importance because the strip may undergo restoration processes during this time. However, owing to the various parts of the strip (the head, tail and midsection) spending different amounts of time within the furnaces, they do not undergo restoration processes at the same rate[2].

Advantages of a Steckel Mill

The two main advantages of a steckel mill are its low cost and the fact that it can be adapted to produce sheet material from metals such as brass. Therefore, it is a worthwhile investment. However, it has other advantages. Thinner gauge lengths can be produced by maintaining a strip at high temperatures, through the use of coiler furnaces. Also, the amount of land required to set up shop is minimised, owing to the presence of the coil boxes, which eliminate the need for long runoff tables, as is the case with a tandem mill. Finally, in addition to producing sheet with a

high quality finish, the steckel is also capable of producing 1.2 million tons of stainless sheets per year.

(a)

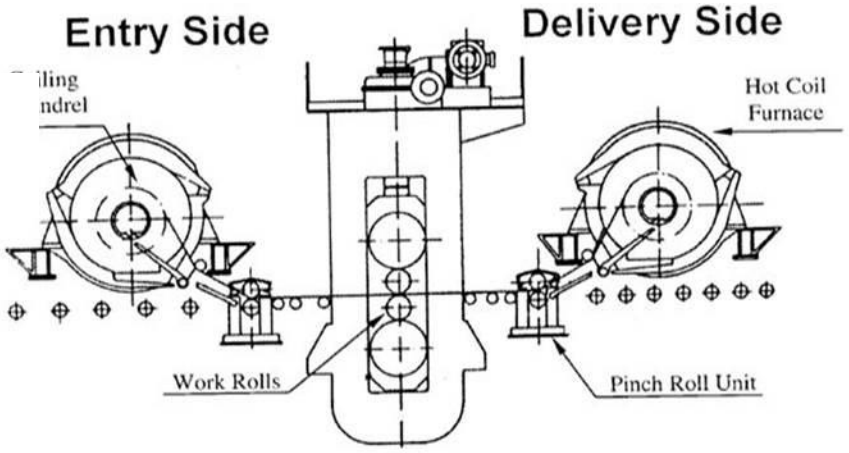

(b)

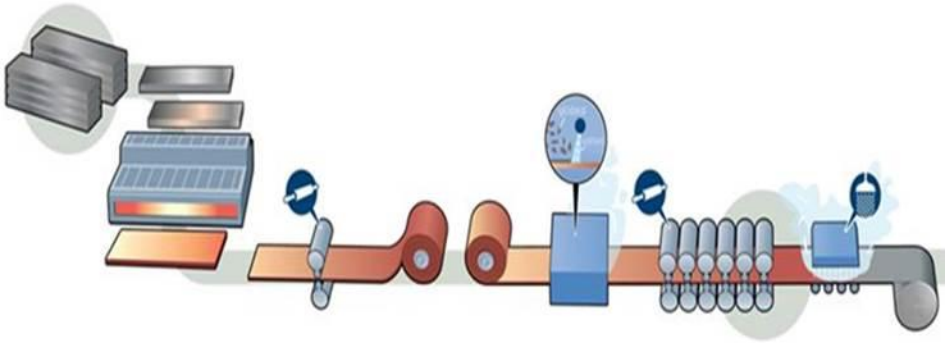

Figure 22. (a) A steckel mill, and (b) a traditional rolling mill[2],[34].

3. EXPERIMENTAL METHOD

3.1 Material

The material used in these experiments consisted of five wrought extra-low interstitial (ELI) Ti-6Al-4V rods with an oxygen content ≤ 0.13%. These rods were10mm diameter and 750mm in length and were machined to 50 cylinders, each with a diameter of 10mm and a length of 15mm. The ends of the samples were surface ground after machining to ensure that the contact faces had a good surface finish.

3.2 Uniaxial testing

3.2.1 Tests Parameters:

The tests carried out in this project focused only on the mid-section of the strip and a three-pass schedule. These tests were done using the parameters shown in **Table 2**.

Table 2. Parameters used during the uniaxial compression tests.

Temperature (°C)	Nominal Strain	Strain Rate (s-1)
850, 950, 1050	0.48	1, 10

Interpass Time

The interpass time is defined as the time that the mill strip spends in the furnace between deformations. It is an important parameter, since during this time the strip may undergo restoration mechanisms, such as recovery or recrystallisation. As mill logs used in multiple deformation schedules of Ti-6Al-4V could not be found, the interpass time was calculated using the mill logs for steckel mill rolling of stainless steels provided by Columbus Stainless Steel.

The initial dimensions of a slab of Ti-6Al-4V were as follows[35]:

Length = 2.5m

Width = 0.95m

Height = 0.2m

From these dimensions, a volume of $0.45m^3$ was obtained. However, before the slab could undergo steckel mill rolling it had to go through a roughing mill, where the height would be reduced to 0.025m. Despite the height reduction, the volume remained constant. Thus, the new dimensions of the slab were as follows:

Length = 20m

Width = 0.95m

Height = 0.025m

Using **Equation 2**, the thickness of the strip after each pass was calculated. The thicknesses, together with the length of the strips after each pass, are presented in **Table 3**.

$$\varepsilon_n = \frac{2}{\sqrt{3}} \ln \frac{h_i}{h_0} \qquad \textbf{Equation 2}$$

where: h_i is the final height and h_o is initial height.

Table 3. The lengths and thicknesses of a Ti-6Al-4V strip during steckel mill rolling.

	Length (m)	**Thickness (m)**
L_1	20	0.025
L_2	30.4	0.016
L_3	46.1	0.011
L_4	69.8	0.0072

Once the thickness during each pass had been obtained, the arc length (L_p) of the rolls could be calculated, using **Equation 3**:

$$L_p = \sqrt{R}(h_0 - h_f) \qquad \textbf{Equation 3}$$

where: R is the work roll radius. (This was given as 0.36 m by Columbus Stainless Steel.)

Using the arc length of the rolls, the roll speed was calculated, using **Equation 4**

$$\varepsilon = \frac{\dot{\varepsilon} \times v}{L_p} \qquad \textbf{Equation 4}$$

where: $\dot{\varepsilon}$ is the strain rate, v is the roll speed and L_p is the arc length of the work roll.

The roll time was then calculated, using **Equation 5**:

$$Rolling\ time = length \times roll\ speed \qquad \textbf{Equation 5}$$

The calculated times for each strain rate are presented in the table below:

Table 4. Roll times calculated for each strain rate.

Time to pass through work rolls at 1/s (s)	**Time to pass through work rolls at 10/s (s)**
263.9	26.3
492.4	49.2
918.7	91.8

For the mid-section of a strip undergoing steckel mill rolling, the interpass time was calculated by taking an average of the consecutive rolls times and adding six seconds. These six seconds accounted for the time it took for the roll gap to adjust between passes. At a strain rate of 1/s, the

interpass times were calculated and found to be 384s and 712s, while at a strain rate of 10/s, the interpass times were calculated to be 44s and 77s, as summarised in **Table 5**.

Table 5. Interpass times used during testing.

Pass	Strain (/s)	Time (s)	Strain (/s)	Time (s)
1-2	1	384	10	44
2-3	1	712	10	77

3.3 Sample Preparation for Uniaxial Compression

The samples used in these experiments were deformed, using Gleeble 3800. The Gleeble 3800 is a computer-controlled thermomechanical simulator that makes use of resistance heating to achieve rapid heating rates up to 10000^0C/s. The temperature of each sample was monitored using thermocouples welded to the centre of the sample by means of percussion welding. The wires were welded in such a way that they were not more than two wire diameters apart, to ensure the accurate measurement of temperature during testing. During testing, it was vital that the thermocouple wires not come into contact with one another, as this would have caused a short circuit. To circumvent this, a ceramic sheath was used.

For these compression tests, an S-type (Platinum, Platinum/Rhodium) thermocouple was used. To weld thermocouple wires on to the specimens, a voltage of 37mV was applied. Furthermore, to lessen the friction between the sample and anvils and to thwart the welding of the sample to the anvils, graphite paper was attached to the ends of the cylinder using nickel paste which also served as lubricant. A coat of nickel paste was also applied to the compression anvils.

Hot deformation was achieved using an argon atmosphere to prevent oxidation. Also, an argon atmosphere was chosen because Ti-6Al-4V samples self-deform when tests are performed under vacuum. Once specimen preparation was complete, the sample appeared as shown in **Figure 23** (a). After the deformation, the samples were air quenched for 60s.

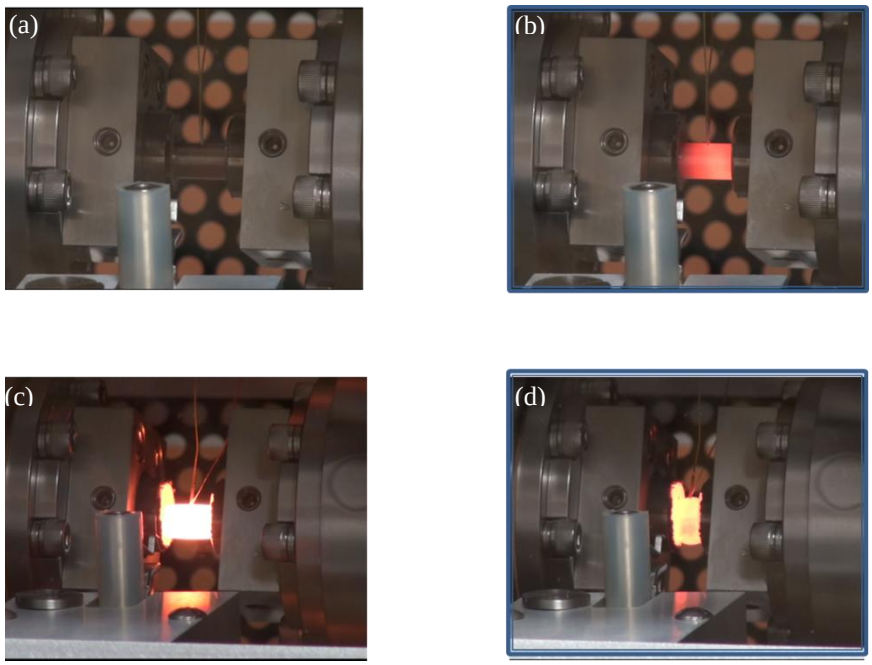

Figure 23. Ti-6Al-4V undergoing deformation in the Gleeble 3800 (a) Sample after being loaded in between anvils, (b) Heating up of sample (c)Sample just before deformation (d) Deformed sample.

The tests were performed using a three-pass (three-hits) multi-deformation schedule. However, for ease of microstructural analysis between passes, the tests were carried out in an interrupted manner, outlined as follows:

- For one hit at any of the test temperatures, the sample was heated at 4°C/s and held at temperature for 30 seconds to allow for homogenisation of the microstructure. The sample was then deformed and air quenched for 60s.

- For two successive hits, a fresh sample was heated to temperature as in the first pass, homogenised for 30 seconds and then deformed. Following deformation, the sample was held at temperature for the interpass time corresponding to the strain rate used, for example, 44s when a strain rate of 10/s was used and 312s when a strain rate of 1/s was used. The sample was then deformed and air quenched for 60s.

- To attain a full three-hits schedule, the procedure carried out in the first two hits was performed on a freshly-prepared sample. However, following the second pass, the sample

was annealed at deformation temperature for either 77s or 712s, depending on the strain rate used. Once the interpass time was reached, the sample was compressed and then air quenched for 60s.

Figure 24 shows the deformation schedule used when Ti-6Al-4V was compressed at 1050°C and a strain rate of 10/s.

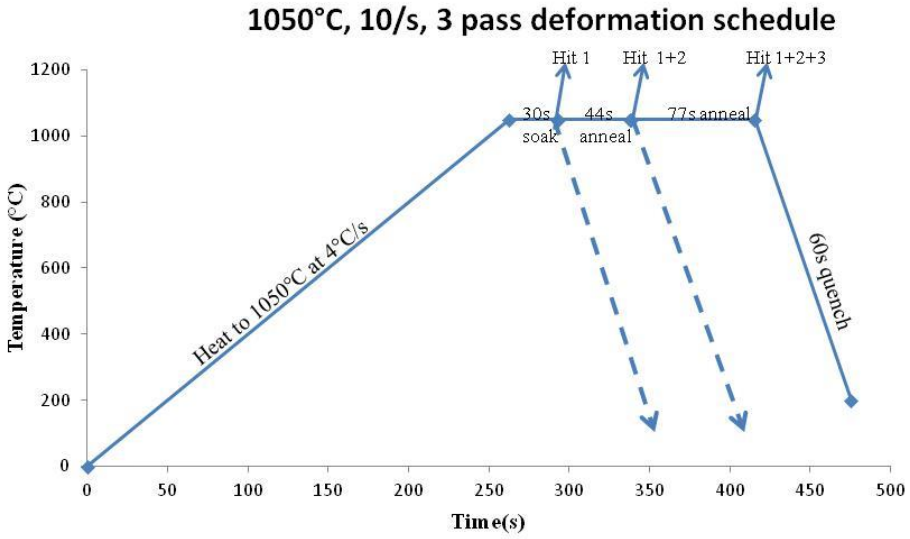

Figure 24. The deformation protocol used on Ti-6Al-4V for compression tests carried out at 1050°C, 10/s.

3.4 Analysis of Variance (ANOVA) and the Taguchi Method

In designing the experiments the Taguchi method was employed to encompass all the parameters and ensure that the experiments were kept to a minimum. A signal to noise (S/N) ratio was then used to analyse the results, in order to determine how much the experimental results deviated from the ideal[36]. For these experiments, a "larger the better" ratio with the following formula was used:

$$S/_N = -10 \log \frac{1}{n} \sum_{i=1}^{n} \frac{1}{y^2}$$ **Equation 6**

Here, n is the total number of tests and y the flow stress value. From this ratio, the optimum processing parameters for the multipass deformation of Ti-6Al-4V could be determined. The influence of each parameter, temperature or strain rate could then be determined using this ratio, as well as ANOVA.

To generate a Taguchi experimental matrix, the three temperatures, 850°C, 950°C, 1050°C were denoted 1, 2 and 3 and the two strain rates, 1/s and 10/s denoted 1 and 2, respectively. **Table 6** shows the resultant L_6 orthogonal array, generated using the Taguchi method. Each paired experiment was repeated three times making a total of 18 experiments.

Table 6. An L_6 orthogonal array for uniaxial compression experiments in the Gleeble 3800.

Experiment number	Temperature	Strain Rate
1	1	1
2	2	1
3	3	1
4	1	2
5	2	2
6	3	2

3.5 Microstructural Analysis

3.5.1 Grinding and Polishing

After deformation, the samples were prepared for microstructural analysis. First, they were sectioned in half, parallel to the compression axis, using an Isomet microslicer. [**Figure 25** (a)] shows where a sample that has undergone one pass at 1050°C has been sectioned longitudinally. It is the centre of this sectioned sample (marked with a square) that is analysed microscopically. During uniaxial compression, friction between the anvils and the sample occurs. The plastic flow of the sample near the contact surface is thus restricted, and the strain at the ends of the sample is lower (approximately equal to the elastic strain)[37] than at the sample's center, which will experience strain greater than the nominal value[38] (0.48 in these experiments). This mid portion of the sample can then be said to under uniaxial strain, whilst the rest of the sample will tend to radiate outwards in a process known as barreling. With an increase in temperature, barreling is lessened and the strain distribution tends to be more uniform. However, with a decrease in strain rate friction between the ends of the sample and the anvils increases, thus the strain at the center of the sample will be higher. Finally, the application of higher strains will also lead to a higher incidence of barreling, that is, the center of the sample will experience strain > than the nominal strain. [**Figure 25**(b)] shows the strain distribution in a modeled simulation of stainless steel, where the compression axis is vertical. The strain distribution depicted in this simulation is typical of all metals that have undergone uniaxial compression. The strain lines are horizontal where the strain concentration is highest: in the middle of the sample.

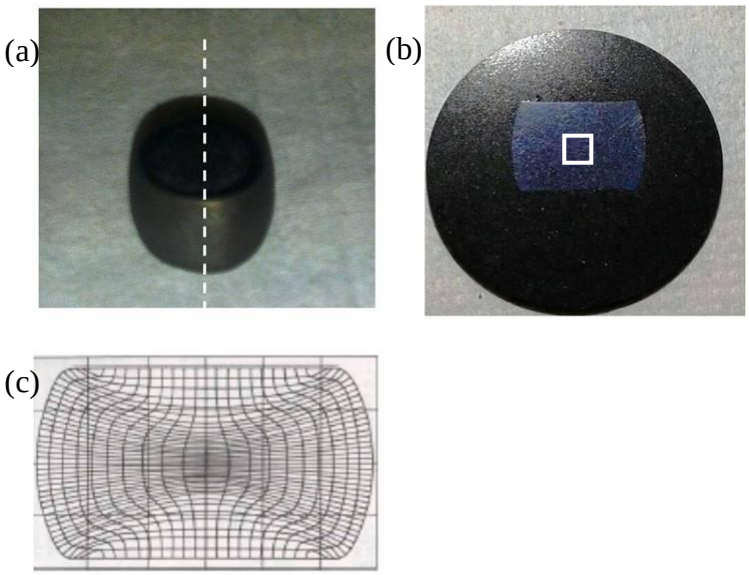

Figure 25. (a) Sectioning of a deformed sample down the middle of the sample, parallel to the compression axis (dotted line), (b) the area where a mounted and etched sample is analysed (white square), and (c) the strain distribution in a model simulation of stainless steel that has undergone a 50% height reduction[39].

The samples were hot mounted, using conductive carbon resin in a Struers Labo-Press 3 set to 180°C, a force of 20kN and a total time of 12 minutes. This time encompassed both heating and cooling cycles. Mounted samples were then ground by hand, using 800 SiC grit paper on a StruersLabo-Pol 25 to remove the rough surface incurred from the cutting of the samples. Following this, a MD-Nap pad was affixed onto a Struers Tegrapol-11 and the samples were automatically polished, using OP colloidal silica, for 30 minutes. This was to eliminate scratches acquired from the grinding of the samples and also to give them a mirror surface finish. Using the same pad, the samples were rinsed with water for 15 minutes.

3.5.2 Scanning Electron Microscopy (SEM)

Piranha solution was used to etch the samples after polishing which was made using H_2SO_4 and H_2O_2 in a 1:1 ratio. In these experiments, 50 ml of H_2O_2 was added to a beaker containing 50 ml of H_2SO_4, using a pipette dropper. This was done under a fume hood. Samples, still mounted in resin, were then immersed in this solution for two hours. Once etching was complete, the

samples were transferred into another beaker, containing clean water, for 20 minutes. This was in order to neutralise the etchant and to clean the samples. Ethanol was used to rinse the samples and they were dried with hot air. Scanning electron microscopy (SEM) was carried out, using an FEI NovaNano SEM 230 at the University of Cape Town. An accelerating voltage of 20 keV, working distance of 8 mm and a current of 0.45nA were used. In the instance, where SEM was coupled with energy dispersive X-ray spectroscopy (EDS), the working distance was changed to 6 mm.

3.5.3 Electron Backscatter Diffraction (EBSD)

The FEI NovaNano SEM 230 was also used to carry out EBSD. Sample preparation was the same as outlined earlier, with the exception that the samples were not etched following polishing. An EBSD detector, set at a working distance of 163mm, was inserted and Oxford HKL Channel 5 Flamenco software was used to capture the EBSD image. The sample was set at a working distance of 13.3mm, the voltage maintained at 20keV, the spot size at 4.5 and the sample set at a 70° pre-tilt. A step size of 0.5u̧m was used during the scanning of EBSD images.

HKL software Tango software was used to post-process and analyse maps after acquisition was complete. The post-processing procedure incorporated a cleaning process where non-indexed points were assigned an orientation based on the sharing of at least four neighbours with the same orientation.

3.5.4 Volume fraction of α phase

The volume fraction of α grains after each pass at 950°C, 1/s, 950°C, 10/s and 1050°C, 10/s was calculated, using the systematic point count method detailed in the ASTM E562-11 standard. However, since the microstructure of interest was that highlighted in [**Figure 25** (b)], the number of fields of view (n) used in these calculations was half that outlined in the standard for a 33% relative accuracy in volume fraction.

4. RESULTS AND DISCUSSION

4.1 The as-received microstructure

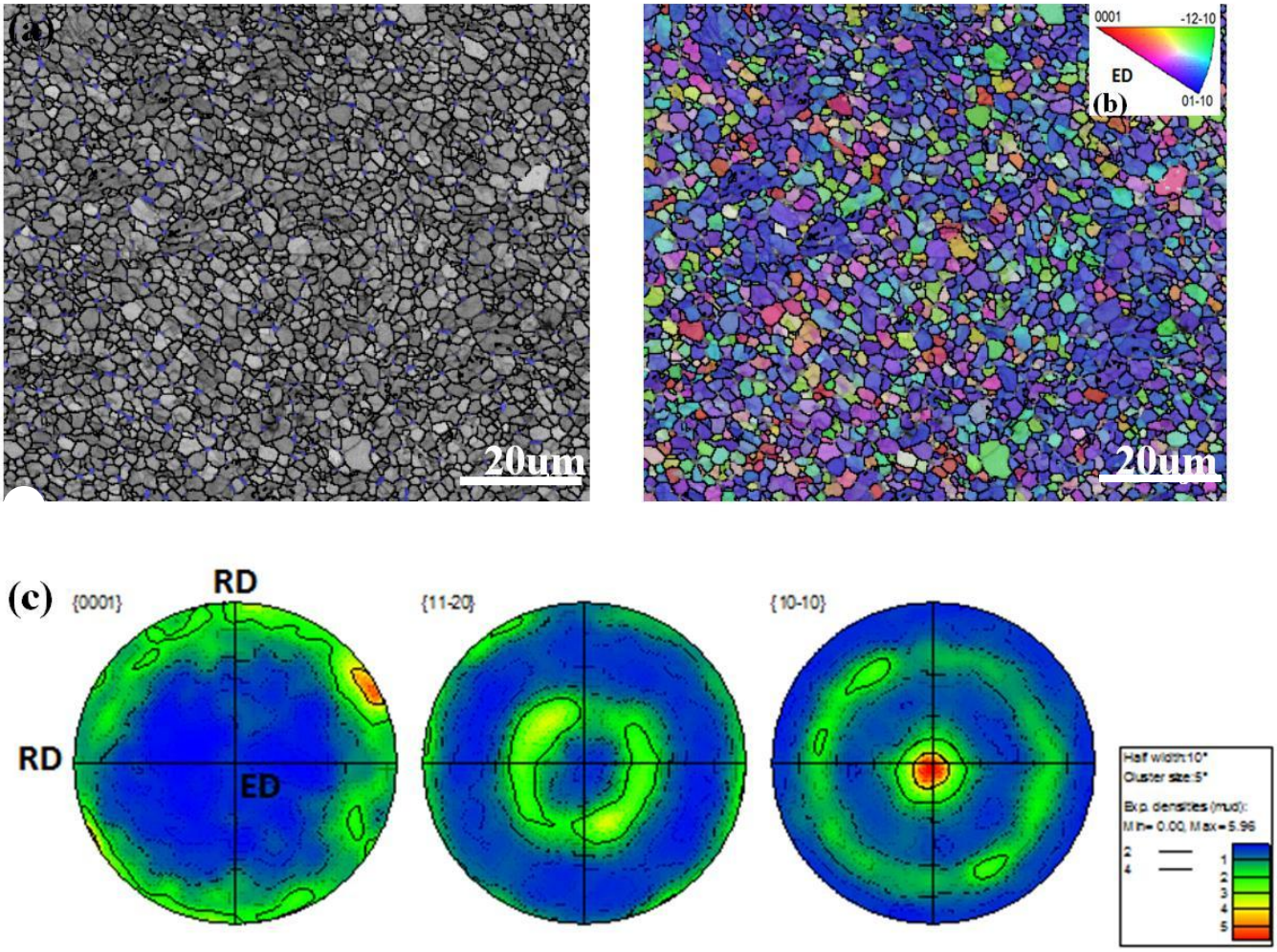

Figure 26. (a) Phase Map overlaid a Band Contrast Map (α phase – grey, β phase - blue), (b) Inverse Pole Figure, (c) $\{\mathbf{0001}\}$, $\{\mathbf{11\bar{2}0}\}$ and $\{\mathbf{10\bar{1}0}\}$ pole figures, (ED- extrusion direction, RD- Radial Direction).

The Ti-6Al-4V rod used in these experiments was extruded at temperatures below the T_β to prevent the formation of a lamellar microstructure. Following this, a recrystallisation heat treatment within the α-β range was carried out for approximately two hours[7]. This resulted in a microstructure consisting of very fine equiaxed α grains approximately 3μm in size. A band

contrast EBSD map of the as-received microstructure is displayed in **Figure 26** (a) and the volume fraction of the β phase (shown in blue) within this rod was found to be between 2-3% using HKL software. It was observed that the β phase was located at the boundaries of the α grains and this served to prevent grain growth during deformation at high temperatures, especially during the process of superplastic forming[6]. This fine, equiaxed microstructure is preferred industrially because it possesses a combination of high strength and ductility in addition to low cycle fatigue strength[40]. The ductility of the equiaxed microstructure in Ti-6Al-4V is enhanced when the grain size is between 1-10μm and the volume fraction of the beta phase is 50% or less[41]. Both these factors promote grain boundary sliding of the α/α interphase during deformation[6,42,43]. The inverse pole figure (IPF), **Figure 26** (b), indicates a strong texture, on which the {10-10} poles are parallel to the extrusion direction, while the basal poles are radially distributed (**Figure 26** (c). This texture is known as {10-10} fiber, and is characteristic of process such as wire drawing and extrusion.

4.2 Microstructure Evolution after Uniaxial Compression

The deformation parameters used during uniaxial compression at 850°C, 950°C and 1050°C are summarised in **Table 7**. Each temperature was assigned two different strain rates, 1/s or 10/s, and to each strain rate a corresponding interpass time. Therefore, at 850°C, for instance, a three-pass schedule at 1/s would have 324s and 712s as interpass times between hits one to two and two to three, respectively.

Table 7. Parameters used during the multipass hot deformation of Ti-6Al-4.

Temperature (°C)	Pass	Strain	Strain rate (/s)	Interpass time (s)	Strain Rate (/s)	Interpass time (s)
850, 950, 1050	1	0.48	1	-	10	-
	1-2	0.48	1	324	10	44
	2-3	0.48	1	712	10	77

4.2.1 Deformation at 850°C,1/s

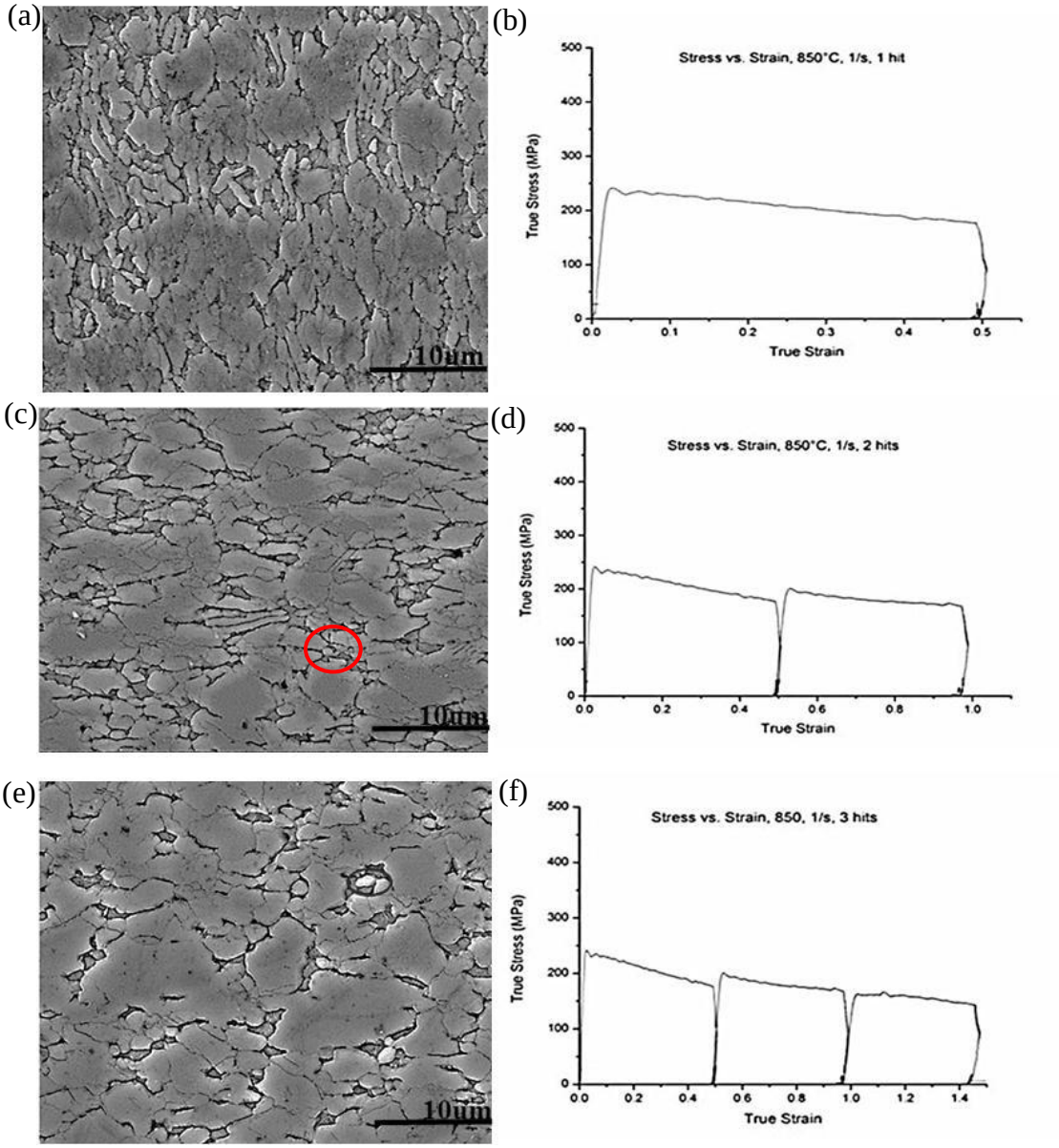

Figure 27. The microstructures (a)-(e) and true stress-true strain curves (b)-(f),depicting flow stress behaviour of Ti-6Al-4V after one, two and three hits at 850°C, 1/s. Circled in (c) and (e) are recrystallised grains formed during hits two and three.

Figure 27 (a) shows that after one hit at 850°C, 1/s, the microstructure consisted of deformed α grains. The true stress-true strain curve in **Figure 27** (b) shows an oscillatory flow stress curve, whose values increased at the onset of deformation. Once a peak flow stress (σ_p) of 240 MPa had

been reached, the flow stress decreased monotonically as deformation proceeded. This behaviour of the flow stress indicated that the microstructure recrystallised partially during uniaxial compression. At the start of deformation, dislocations motion was initiated and dislocation multiplication occurred. The result was work hardening, which raises the stored energy within the material. When a critical strain value (ε_c) of 0.0104 was reached, small, dislocation-free grains nucleated at old grain boundaries and dislocations. This process is known as dynamic recrystallisation (DRX) and is the cause of flow softening during hot deformation[44]. Recrystallisation of Ti-6Al-4V with an equiaxed preform during deformation at 850°C, 1/s has been alluded to by other researchers[6,32,45].

After two successive passes, the microstructure comprised a mixture of coarse, deformed grains, as well as some recrystallised equiaxed grains [circled in **Figure 27** (c)]. These recrystallised grains formed through dynamic recrystallisation. The occurrence of these recrystallised grains was observed at the grain boundaries of deformed grains, which was expected, as grain boundaries are regions of high energy[21]. The coarse grains within the microstructure arose as the sample was being annealed for 324s following the first hit. During this time, the deformed grains from the first pass dissipated stored energy from static recrystallisation[3] and this was followed by grain growth. Moreover, the grains that had dynamically recrystallised during the first hit also underwent grain growth, a process that was inhibited during hot deformation[18,46]. These coarsened grains were then deformed at the second hit and so attained their appearance in **Figure 27** (c).The true stress-true strain curve displays a similar pattern to that of the first pass: work hardening followed by flow softening, owing to dynamic recrystallisation after a maximum flow stress had been attained. Both the peak and average flow stress decreased at this pass, as shown in **Table 8.**

Three successive passes at 850°C, 1/s resulted in a microstructure consisting of coarser deformed grains. In addition, small equiaxed grains were now observed not only at the grain boundaries of the deformed grains, but also between the fine α lamellae within the β phase. One such grain is circled in **Figure 27** (e) and shown in the higher magnification micrograph in **Figure 28**. At 850°C, the β phase was present within the sample at approximately 20%[6]. Hence, when the sample was quenched to room temperature after compression, the β phase transformed into lamellar α, which was the stable phase at room temperature.

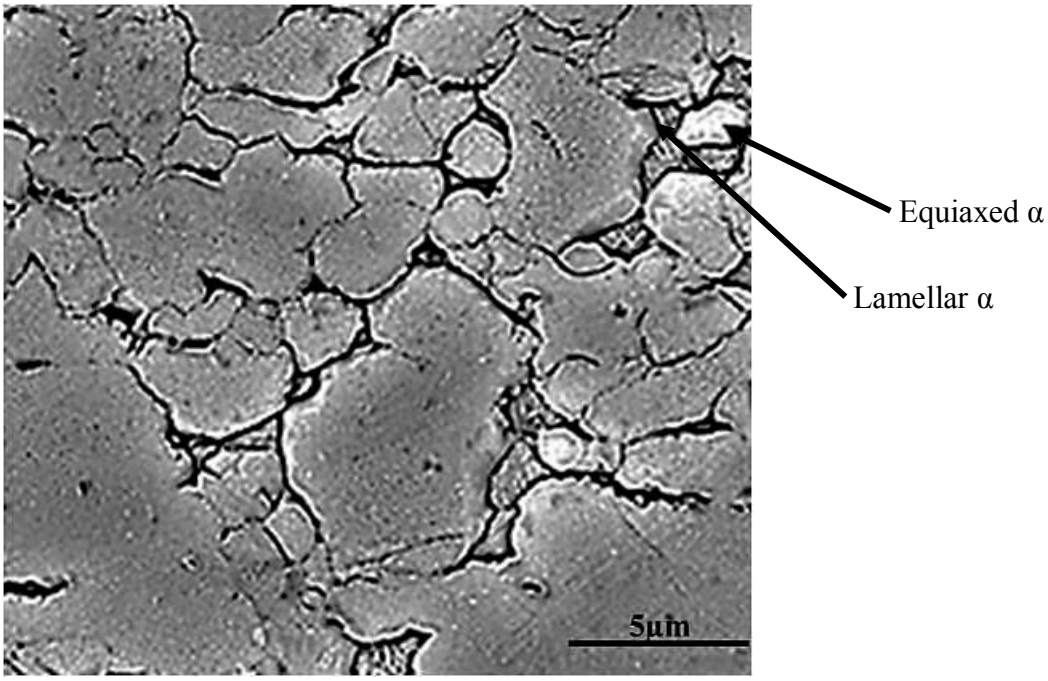

Figure 28. Equiaxed α within lamellar α.

The true stress-true strain curve in **Figure 27** (f) at the third pass exhibits a plateau after a peak strain (ε_p) of 1.12, indicating that the rate of work hardening was now at equilibrium with that of flow softening owing to recrystallisation. In **Table 8** below, the average flow stress is shown to have decreased with each subsequent pass and this was due to the recrystallisation and grain growth that occurred during the interpass times. Also seen in this table are critical stress (σ_c) and critical strain (ε_c), required to initiate recrystallisation during deformation.Values of the σ_c and ε_c were obtained using empirical **Equation 6**, **Equation 7**[46,47]**.**

$$\varepsilon_c = 0.4_p \qquad \textbf{Equation 7}$$

$$\sigma_p = 0.95_p \qquad \textbf{Equation 8}$$

where σ_p and ε_p are the peak stress and peak strain, respectively.

Table 8. Average flow stress, peak flow stress and strain, as well as critical stress and strain per pass, at 850°C, 1/s.

Hit	Average flow stress (MPa)	Peak flow stress (σ_p)(MPa)	Critical flow stress(σ_c)	Peak Strain (ε_p)	Critical Strain (ε_c)
1	251	240	229	0.0260	0.0104
2	207	200	190	0.533	0.213
3	189	165	157	1.122	0.448

4.2.2 Deformation at 850°C, 10/s

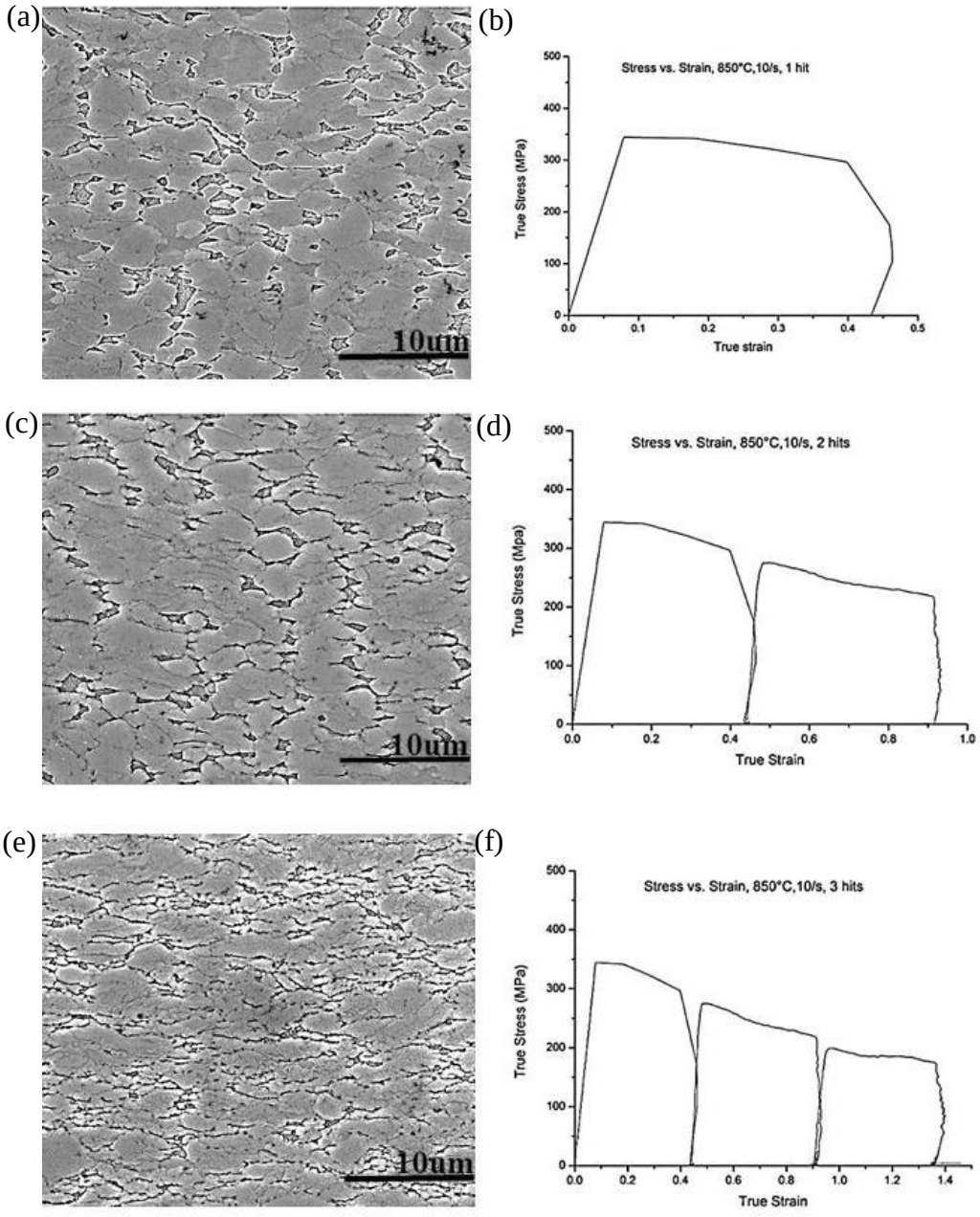

Figure 29. The microstructures (a)-(e) and true stress-true strain (b)- (f) true stress-true strain curves depicting flow stress behaviour of Ti-6Al-4V after one, two and three hits at 850°C, 10/s.

After one hit at 850°C, 10/s, the microstructure is shown in **Figure 29** (a) and it consists of deformed gains. The true stress-true strain curve displayed in **Figure 29** (b) shows an increase in

flow stress owing to work hardening. A plateau is then reached at 354 MPa, after which a dip in flow stress is observed. The plateau in the flow stress curve after one hit at 10/s indicates that the microstructure underwent recovery during hot deformation. This is known as dynamic recovery (DRV) and was to be expected because when the strain rate is increased, dislocation multiplication occurs but its motion limited. Thus, while this temperature was sufficient to allow for the formation of lower energy polygonised subgrains, it was insufficient for their migration. Therefore, the greater than 10° misorientation angle between subgrains that is required to form high angle grain boundaries was not achieved. It is the region between these high angle grain boundaries that serves as a nucleus for recystallised grains[46]. However, the formation of subgrains does not alter the shape of the grains, so they retain their deformed shape. The slight dip in flow stress seen after the plateau in the figure is indicative of adiabatic heating, caused by hot working at high strain rates[18,20].

The true stress-true strain curve in **Figure 29** (d) shows that, following an inter-anneal time of 44s, the flow stress was now lower than at hit one [**Table 9**] and this was due to recrystallisation and grain growth occurring during the interpass time of 44s, prior to the second hit. Since the distribution of strain was non-uniform at this strain rate, it followed that recrystallisation and grain growth would be non-uniform, occurring where the dislocation density was at its highest. Following two hot compressions, the sample was annealed for 77s at the deformation temperature, after which steady state was observed in the flow stress curve [**Figure 29** (f)]. This was a result of the rate of work hardening being equal to that of flow softening.

Table 9. Average flow stress, peak flow stress and strain, as well as critical stress and strain per pass at 850, 10/s.

Hit	Average flow stress (MPa)	Peak flow stress (σ_p)(MPa)	Critical flow stress (σ_c)	Peak Strain (ε_p)	Critical Strain (ε_c)
1	313	354	336	0.167	0.067
2	235	271	257	0.485	0.194
3	201	197	187	0.979	0.392

4.2.3 Summary

The graph in **Figure 30** shows that the average flow stress increased with an increase in strain rate, as was expected. However, contrary to expectations, recrystallisation at the higher strain rate was less than that at 1/s. This was due to the uneven distribution in strain at the 10/s which resulted in the recrystallisation itself being heterogeneous. The higher interpass times that arose from the use of a low strain further served to promote recrystallisation at this temperature, but this benefit was counteracted by grain growth.

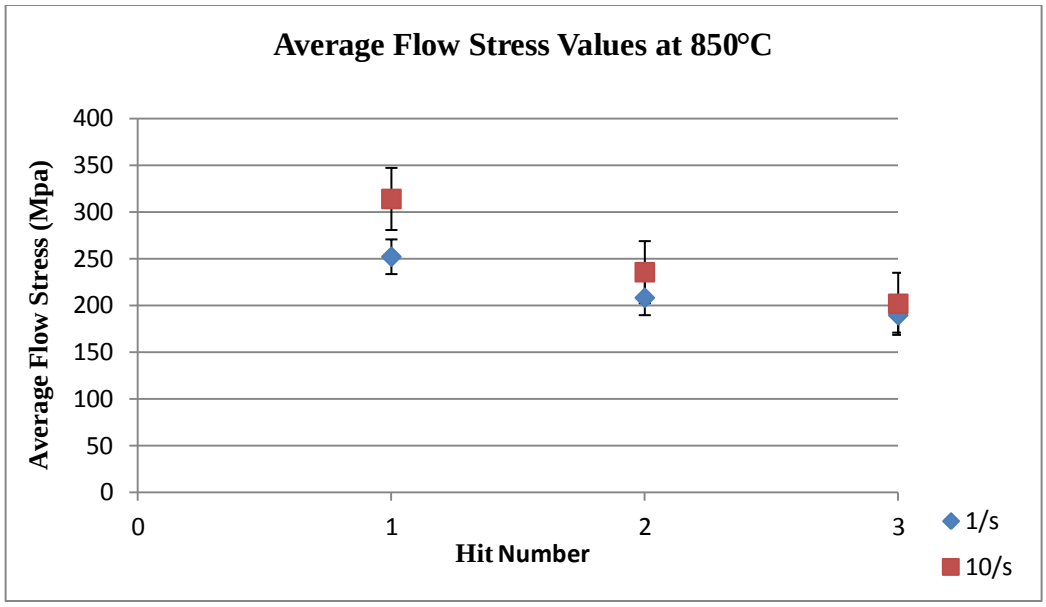

Figure 30. Graph of average flow stress values against pass number at 850°C, 1/s and 850°C, 10/s.

4.2.4 Deformation at 950, 1/s

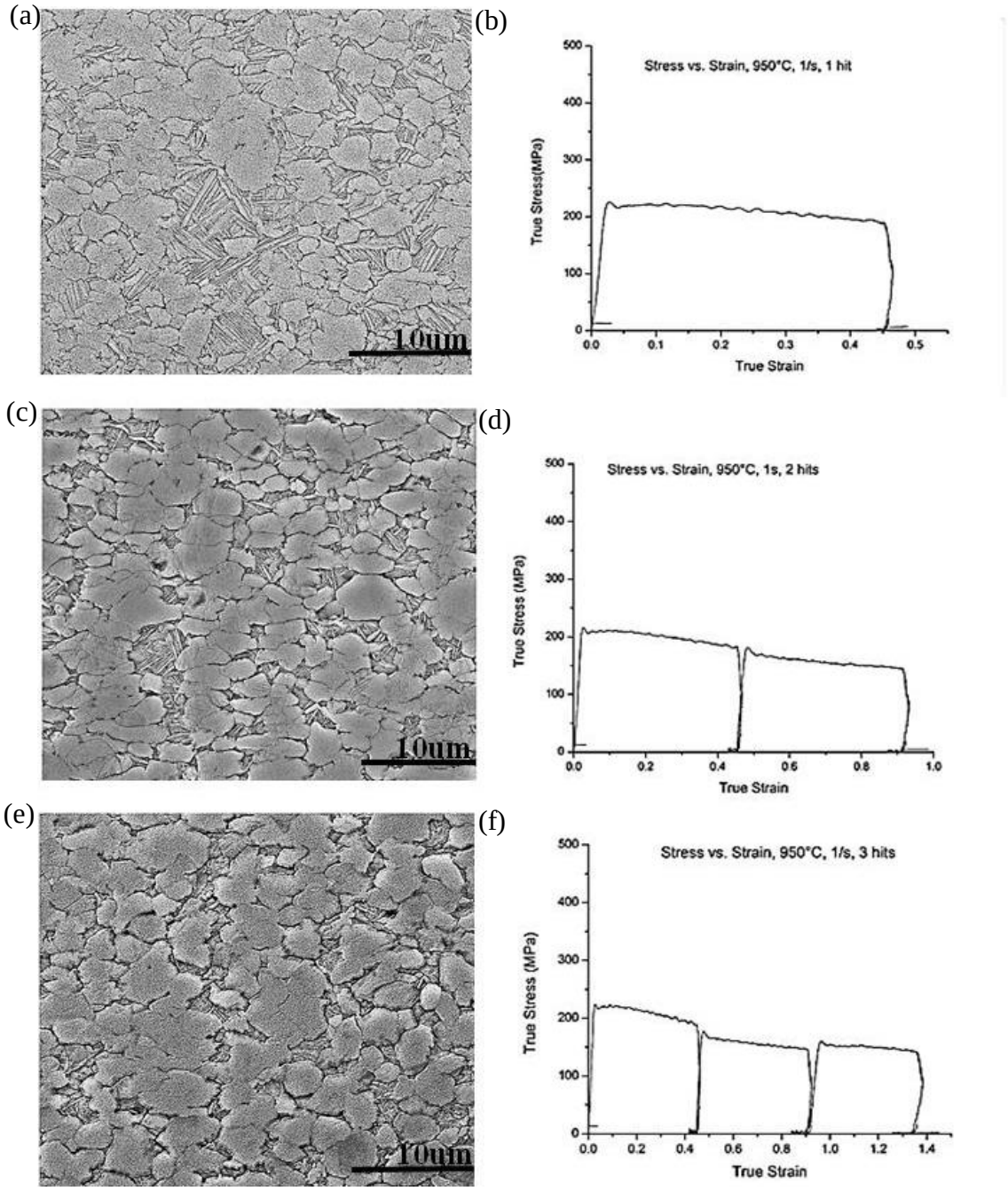

Figure 31. (a)-(e) The microstructures and (b)-(f) true stress-true strain curves, depicting flow stress behaviour of Ti-6Al-4V after one, two and three hits at 950°C, 1/s.

The true stress-true strain curve [**Figure 31** (b)], after a single hit at 950°C, 1/s, shows an increase in flow stress at the start of deformation. A maximum flow stress was then reached at

233 MPa and was followed by continuous flow softening. This trend had been observed during the hot deformation of Ti-6Al-4V at this temperature and strain rate and the phenomenon attributed to globularisation ofTi-6Al-4V, with either fully lamellar or bi-modal preforms[6,30,43,48,49]. However, as shown by **Figure 26**, the initial microstructure of the Ti-6Al-4V used in this project was equiaxed with no α lamellae. Consequently, when the alloy was heated to 950°C, some of the primary α (α_p) phase transformed into β, resulting in a microstructure consisting of both α_p and β phase, whose volume fraction was approximately 60% [6]. Deformation of the sample resulted in the movement and multiplication of dislocations, which resulted in work hardening and an increase of stored energy. When a critical strain of approximately 0.012 was reached, a phase transformation took place. Such a transformation would have occurred during deformation, as well as during the interpass time, when the sample was annealed at deformation temperature for 324s. Microstructural defects, such as dislocations, raised the stored energy of the material, thereby driving the transformation from β phase to α once a critical strain had been reached. The process by which β phase is transformed to thermodynamically stable equiaxed α during deformation is known as a strain-induced phase transformation (SIT)[48,50] and was observed by Dehghan-Manshadi *et al.*[51] during compression tests on α-β alloy Ti-6Al-2Sn-4Zr-2Mo. Following deformation, the alloy was quenched, resulting in transformation of β phase into α_w. The resultant microstructure was bi-modal (equiaxed α grains separated by equilibrium α+β lamellae, with Widmanstätten morphology) and is shown in **Figure 31** (b). This microstructure was different from findings by Dehghan-Manshadi *et al.* and He *et al.*, where β phase transformed into martensite upon quenching, following hot deformation at sub-transus temperatures[50,51]. The reason for this can be ascribed either to the varying quench rates used (14°C/s in these experiments vs. 500°C/s used in the researchers' experiments) or to the fact that, in the case of Dehghan-Manshadi *et al.*, the alloy was Ti-6Al-2Sn-4Zr-2Mo,the composition of which is different from that of Ti-6Al-4V.

The microstructure after the second pass is displayed in **Figure 31** (c) and it consists of coarse deformed α grains, as well asWidmanstätten α+β lamellae. The number of equiaxed α grains in this microstructure [**Figure 31** (c)] appears to have increased in comparison to those after the first hit [**Table 11**]. The decrease in lamellar α indicates that the β phase continued to transform into globular α when deformation was ceased, with the dislocations at β grain boundaries and

within β grains serving as sites for nucleation and growth. Meanwhile, those grains that nucleated during deformation grew.

The effect of temperature was also considered, that is, whether the SIT from β phase into α was not due to a decrease in temperature during either deformation or inter-annealing. A graph of temperature against time was then plotted [**Figure 32** (a)]. **Figure 32** (b) is a close-up of **Figure 32** (a) at hits one and two and it shows that the temperature was stable at interpass times and only increased when the sample was deformed, where a sharp spike was observed. Since heat is muted during deformation, the Gleeble must readjust/ recalibrate to the temperature of the sample just after deformation and this presents as sharp rise in temperature, which is followed by a sharp drop. This occurred quickly, as shown in **Figure 32** (b), and would not have provided sufficient time for a phase transformation. Following this brief fluctuation, the temperature then stabilised and it was this stabilisation that showed that the phase transformation was brought about by strain and not influenced by temperature instability.

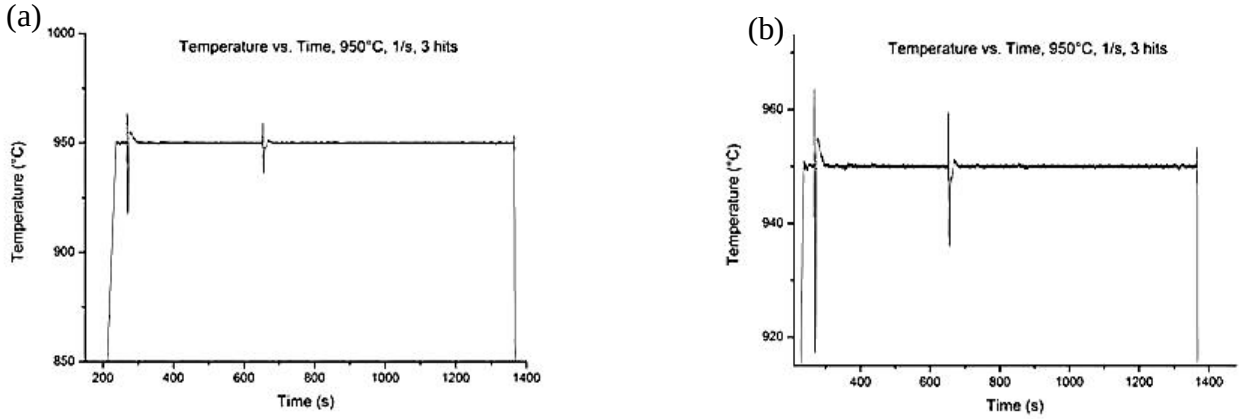

Figure 32. Temperature-time graph after 3 hits at 950°C, 1/s.

Table 10 shows that, as a consequence of the increase in the number of α grains, as well as their coarsening during the interpass time, the average flow stress decreased from 201MPa at pass one to159 MPa at the second pass [**Table 10**]. This decrease was in agreement with studies by Park *et al.*[32], who found that a microstructure consisting of equiaxed α was softer and would thus display lower flow stress values in comparison to its bimodal counterpart. The true stress-true strain curve at the second pass had a similar appearance to that of the first pass: work hardening

due to the motion and multiplication of dislocations, and flow softening due to the SIT of the β phase.

Three successive hits at 950°C, 1/s resulted in a microstructure that also consisted of coarse, deformed grains [**Figure 31** (e)]. In **Table 11**, it can be seen that the volume fraction of α grains increased further, as more beta β was transformed into α during the 712s interpass time. At the third hit, once a critical strain of 0.39 had been exceeded [**Figure 31** (f)], the true stress-true strain curve was steady state, as equilibrium had been reached between work hardening and flow softening. The average flow stress at this pass was 159MPa, which was similar to that at the second pass.

Table 10. Average flow stress, peak flow stress and strain, as well as critical stress and strain per pass at 950, 1/s.

Hit	Average flow stress (MPa)	Peak flow stress (σ_p)(MPa)	Critical flow stress (σ_c)	Peak Strain(ε_p)	Critical Strain (ε_c)
1	201	236	224	0.030	0.012
2	159	198	189	0.48	0.19
3	159	174	165	0.97	0.39

Table 11. Volume fractions of equiaxed α grains after each pass at 950°C, 1/s.

Hit	Volume fraction of α grains	standard deviation
1	55	3.61
2	62.5	3.54
3	67	3.46

4.2.5 Deformation at 950°C, 10/s

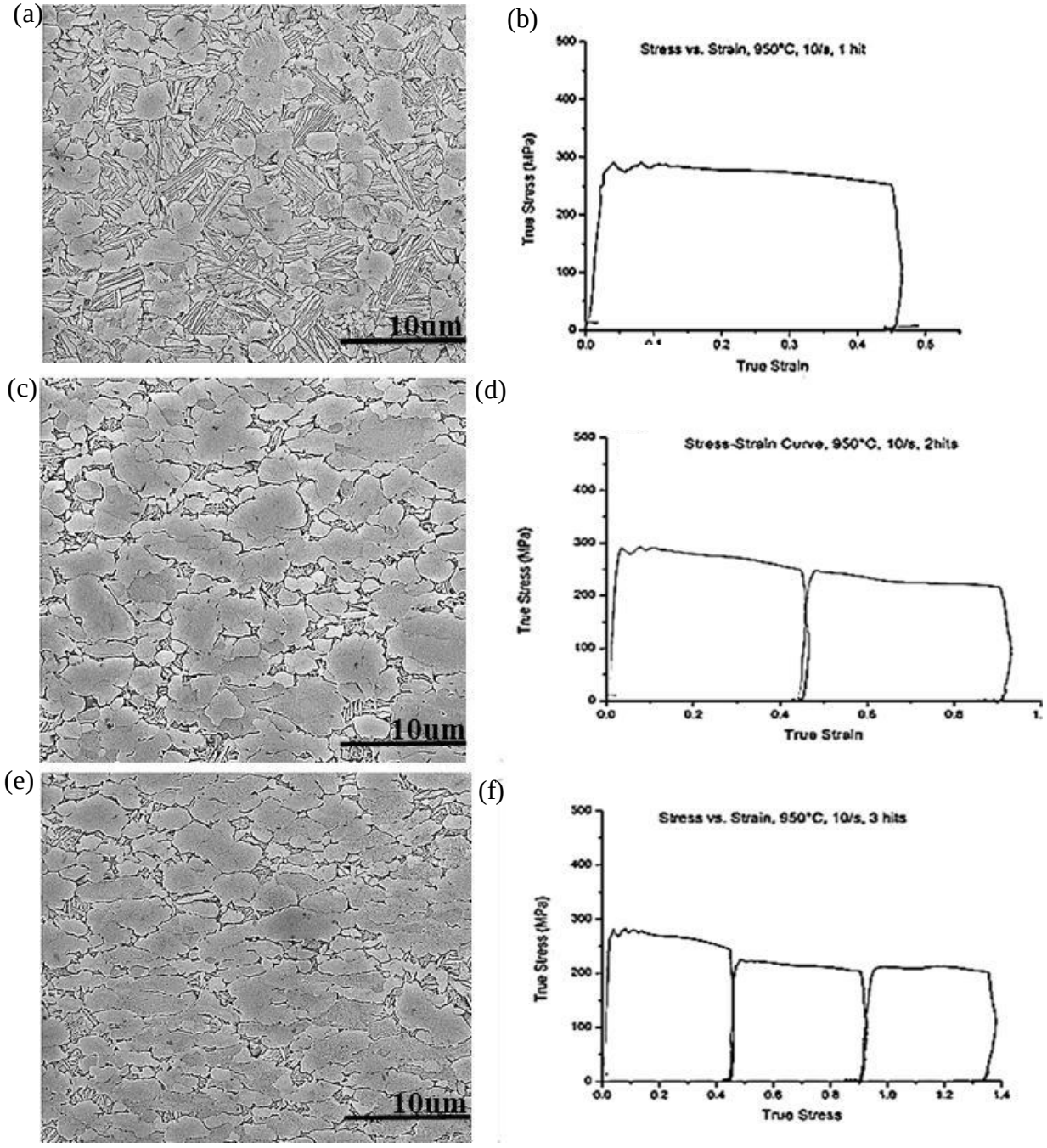

Figure 33. The microstructures (a)- (e) and true stress-true strain (b)-(f) true stress-true strain curves, depicting flow stress behaviour of Ti-6Al-4V after one, two and three hits at 950°C, 10/s.

After one pass at 950°C, 10/s the microstructure was bi-modal [**Figure 33** (a)]. Table 13 shows the volume fraction of α grains within the microstructure, following deformation of Ti-6Al-4V at

each pass. From this table, it can be observed that the volume fraction of the lamellar phase after the first pass was 58.5%, which was approximately 13.5% higher than the volume fraction within the microstructure at 950°C, 1/s. **Figure 34** shows temperature fluctuations after the first hit and, unlike those seen at a similar point at 950°C, 1/s, these persisted for longer, with the temperature being as high as 978°C, whereas it should have stabilised to 950°C.This might have led to adiabatic heating within the sample and thus led to the increasing of the volume fraction of the β phase. On air quenching of the sample, the β phase was transformed into α lamellae.

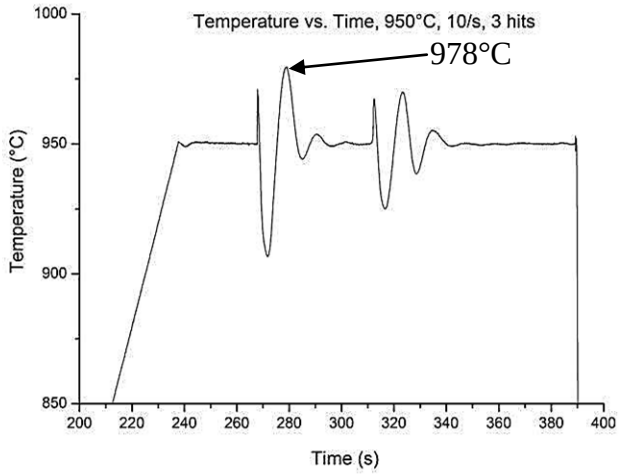

Figure 34. Temperature-time graph after three hits at 950°C, 10/s.

In addition, further study of this microstructure revealed that the equiaxed α grains at this strain rate were slightly finer than those of the sample deformed at 950°C, 1/s. The linear intercept method was used to calculate the grain size and it was found to be approximately 7.53 μm after one hit at 1/s whereas after one hit at 10/s, it was 6.80 μm. Although an increase in strain rate is known to bring about an increase in the flow stress due to the increase in the velocity of dislocations[52],it is also thought to bring about the refinement of grain size[21,46,50]. This is by increasing the dislocation density although the mechanism of this increase is not understood. These now denser dislocations then serve as sites for the nucleation of α grains. Furthermore, at a higher strain rate, the sample spends less time at temperature during deformation and this also contributes to the finer grain size. As was the case at the first pass at 950°C, 1/s, flow softening, following a maximum flow stress, was seen in the true stress-true strain curve [**Figure 33** (b)]

and it was also due to the SIT of the β phase. However, the flow stress curve at this strain rate had jagged points at the onset of compression. These were due to flow instability, caused by resistance to dislocation movement, a consequence of using a high strain rate. Once this resistance had been overcome, deformation proceeded smoothly. 0.2% proof stress had to be used in order to acquire the peak flow stress in this instance. The values of the peak flow stress, average flow stress, 0.2% proof stress and critical strain per pass are shown in **Table 12**.

Figure 33 (c) shows the microstructure of Ti-6Al-4V after two successive passes at 950°C, 10/s. This microstructure consisted of deformed globular α grains and some finer, recrystallised equiaxed grains, which arose from SIT during deformation. The volume fraction of the α phase increased to 65% at this pass [**Table 13**] and it was the transformation of the β phase into equiaxed α phase during deformation, as well as during the inter-anneal time of 44s, that was responsible for this. Grain growth also took place, leading to the effective decrease in the average flow stress at the second hit. A further increase in the volume fraction of the equiaxed α phase to 68% was observed after Ti-6Al-4V had undergone three consecutive passes at 950°C, 10/s [**Figure 33** (e),**Table 13**]. This means that when the sample was held at temperature for 77s, there was further transformation of β phase into equiaxed α phase and then grain growth. Fine equiaxed grains in the microstructure were the result of β phase transforming into equiaxed α during deformation. As with the third hit at 1/s, the flow stress curve at the third hit showed steady state behaviour, as the rate of work hardening had reached equilibrium with that of flow softening.

Table 12. Average flow stress, 0.2% proof stress and strain, as well as critical stress and strain per pass, required to initiate restoration mechanisms at 950°C, 10/s.

Hit	Average flow stress (MPa)	0.2% proof stress (σ_p)(MPa)	Critical flow stress (σ_c)	Peak Strain(ε_p)	Critical Strain (ε_c)
1	265	270	276	0.046	0.031
2	232	260	247	0.49	0.19
3	224	249	236	1.05	0.42

Table 13. Volume fractions of equiaxed α grains after each pass at 950°C, 10/s.

Hit	Volume fraction of α grains (%)	Standard deviation
1	41.5	3.81
2	65	3.35
3	68	2.82

4.2.6 Summary

During multi-pass deformation of Ti-6Al-4V at 950°C, it was observed that the flow stress curves exhibited a similar pattern, regardless of strain rate, and work hardening, followed by flow softening, occurred at each pass **[Figure 31** (a)-e) and **Figure 33** (a)-(e)].

Average flow stress values of samples deformed at 950°C, using either 1/s or 10/s strain rates, are shown in **Figure 35**. These values were higher when the sample was deformed at 10/s, although at both strain rates the flow stress decreased at each pass, on account of the strain-induced phase transformation of the β phase. The flow stress being higher at 10/s was due to the velocity of dislocations being higher at a higher strain rate. As a consequence, these dislocations piled up, resulting in a higher force being required in order to enable their motion.

Temperature fluctuations might have led to adiabatic heating occurring during uniaxial compression of Ti-6Al-4V at 950°C, 10/s, resulting in the microstructure consisting of a higher amount of lamellar α phase, in comparison to its 1/s counterpart despite both microstructures being bimodal. Another effect of using a high strain rate was that, with each subsequent pass, the volume fraction of equiaxed α grains also increased. **Table 14** further shows that this increase was more significant at 10/s, as the volume fraction of α grains had increased by 26.5% after three hits, in comparison to the 12% increase at 1/s. The increase in dislocation density, caused

by an increased strain rate, meant that the sites for the nucleation and growth of equiaxed α grains at β grain boundaries, as well as within β grains were also increased.

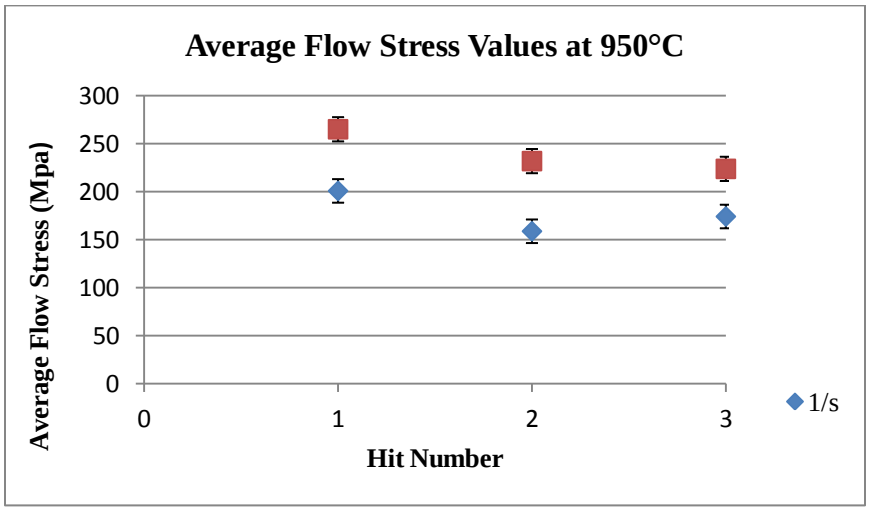

Figure 35. Graph of average flow stress values against pass number at 950°C, 1/s and 950°C, 10/s.

Table 14. The volume fraction of equiaxed α grains at 950°C at either 1/s or 10/s.

Strain rate (/s)	Pass	Volume fraction of equiaxed α grains (%)	Strain Rate (/s)	Pass	Volume fraction of α grains (%)
1	1	55	10	1	41.5
	2	62.5		2	67
	3	67		3	68

4.2.7 Deformation at 1050°C, 1/s

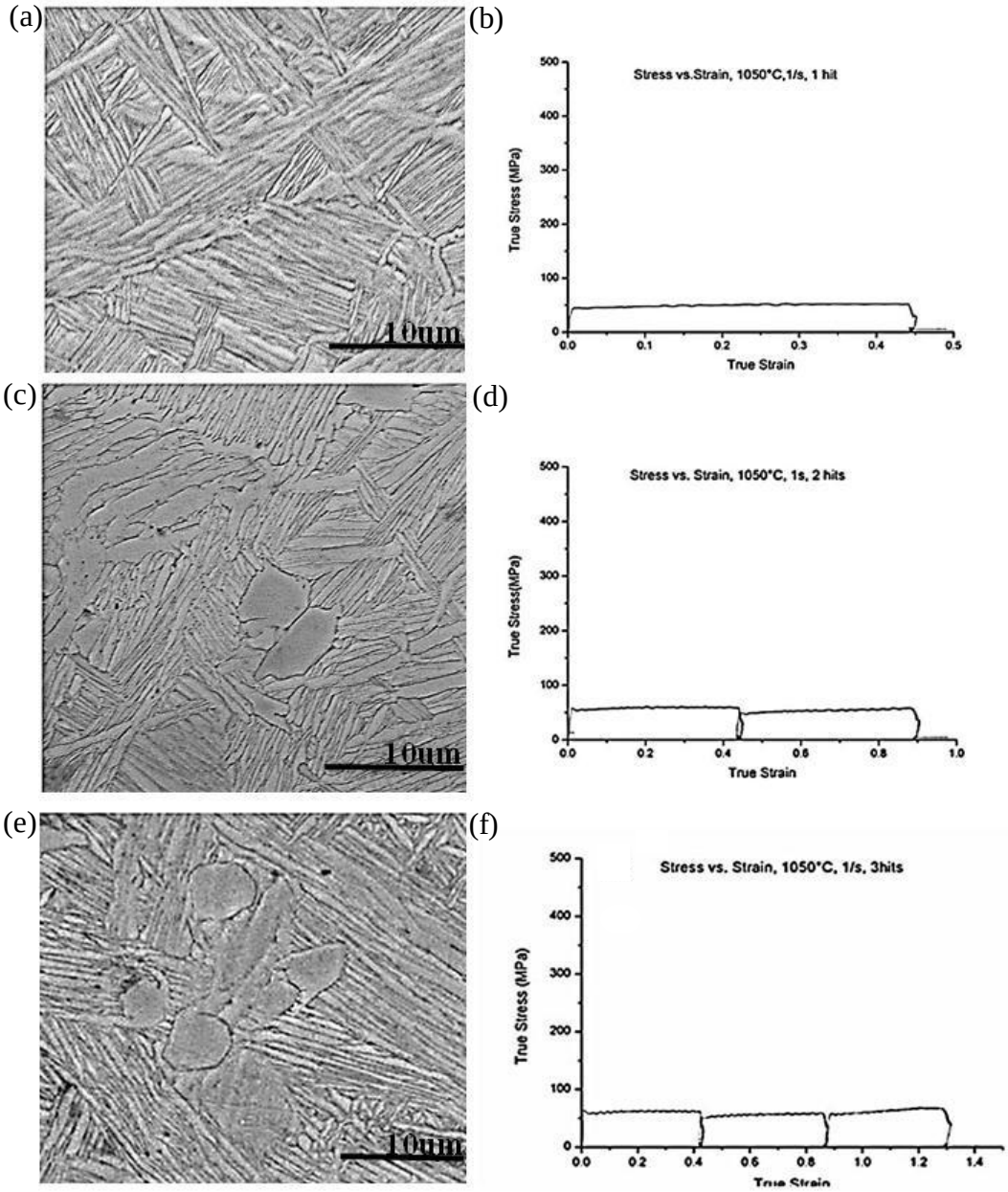

Figure 36. The microstructures (a)-(e) and true stress-true strain (b)- (f) true stress-true strain curves, depicting flow stress behaviour of Ti-6Al-4V after one, two and three hits at 1050°C, 1/s.

A single pass at 1050°C, 1/s resulted in a microstructure consisting of equilibrium α+ β lamellae with Widmanstätten morphology [**Figure 36** (a)]. This microstructure was the result of the alloy being deformed and then quenched from above the T_β. This was in keeping with observations by

S.M. Kelly, who found that the use of an intermediate cooling rate resulted in such a microstructure when Ti-6Al-4V was cooled from above the T_β[8]. At 1050°C, Ti-6Al-4V consisted solely of the β phase and, on quenching; (α_{gb}) formed at prior β grain boundaries. Once the entire prior β grain boundary was covered by α_{gb}, parallel plates of α_w delineated by β phase, then grew into the prior β grain, eventually joining up with other lamellae that grew from other points within the same prior β grain[8]. The flow stress at hit one in the true stress-true strain graph [**Figure 36** (b)] was steady state ,which, coupled with the oscillatory behaviour, indicated that recrystallisation had taken place during deformation[18].These features were borne by all three true stress-true strain curves at this temperature and this was in agreement with work by other researchers[6,24,53] when they carried out uniaxial compression of Ti-6Al-4V under similar conditions. **Table 15** summarises the average flow stress values and also shows the ε_c and σ_p required to initiate recrystallisation at each pass during deformation at 1050°C,1/s.

Despite recrystallisation having taken place, the prior β grain size at this temperature was very coarse following deformation. This, in part, was due to the growth of β grains during the 30s hold prior to the first hit and, also, to the diffusion rate being high with the result that nucleation and growth of recrystallised grains proceeded at a fast rate[46]. Therefore, grain refinement was not possible and the prior β grain size remained coarse.

After two passes at 1050°C, equiaxed α, together with α_w was observed within the microstructure [**Figure 36** (c)]. However, this microstructure was not bimodal. **Table 16** depicts volume fraction of equiaxed α grains after two and three hits. Also, following two hits, the prior β grain size was then so coarse that prior β grain boundaries were barely visible on the micrograph. While recrystallisation resulted in the reduction of stored energy, the grain boundaries were still regions of high energy and were thermodynamically unstable[18].Therefore, during the interpass time of 324s (between hit one and hit two), growth of dynamically recrystallised β grains occurred, in order to further reduce stored energy within the microstructure and attain stability[21].The consequence of grain growth was such that it lowered the flow stress when the alloy was deformed a second time. At this temperature, the strain-induced phase transformation from β phase into α at the deformation temperature was not possible, as the α phase cannot exist above the T_β. Thus, upon quenching of the sample, a SIT from β to equiaxed α could have then occurred where dislocation density within the sample was high. SIT at this temperature was not

as extensive as that observed at 950°C, 1/s. This was due to compression being carried out at both a low strain and a higher temperature, resulting in dislocations being readily annihilated. Consequently, the stored energy within the microstructure was lower and the driving force towards a phase transformation from β to α was reduced. After three consecutive hits, the microstructure was similar to that obtained after two passes. In **Figure 37**, the temperature is shown to be stable throughout all three hits; hence the phase transformation from β phase to equiaxed α cannot be ascribed to a drop in temperature during deformation.

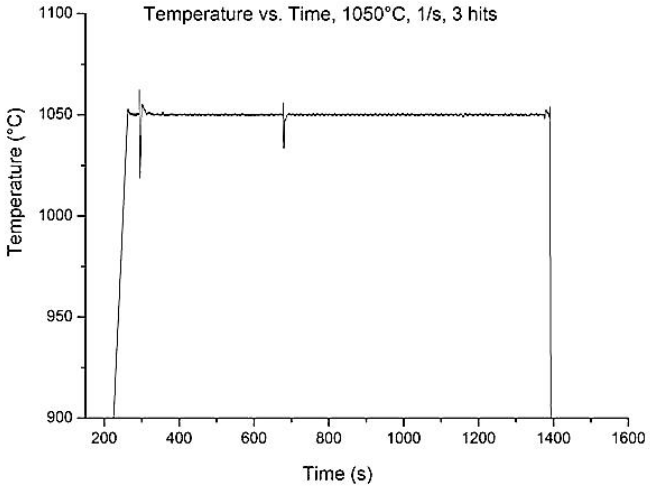

Figure 37. Temperature-time graph after three hits at 1050°C, 1/s.

Energy dispersive X-ray spectroscopy (EDS) in the SEM was used to ascertain the chemical composition of α and β phases. A compositional difference between these two phases would confirm that lamellar α, seen in the micrographs in **Figure 36** (a)-(e), was Widmanstätten and not martensite. The graph in Figure 38 shows the wt% of Al and V, at the points indicated on the image, and it must be noted that the balance was Ti for each spectrum point. In this graph, it is seen that the composition of Al was higher than that of V. This was to be expected for an equilibrium α-β phase, as there was time during cooling for the two elements (Al and V) to separate. If the microstructure had been martensitic, the spectrum would have shown compositional invariance and the microstructure would have consisted of acicular laths, oriented 30, 60 and 90° to one another. Owing to the diffusionless nature of the martensitic

transformation, partitioning of the elements Al and V would not occur, thus the laths are not separated by β phase. In comparison, α_w was delineated by the β phase and the lamellae were parallel one another.

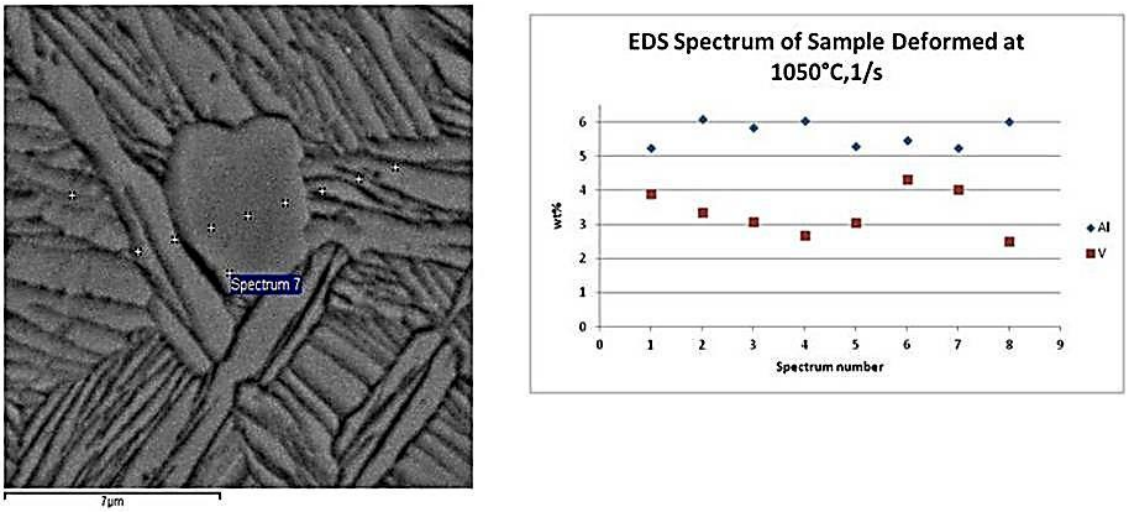

Figure 38. EDS Spectrum of Ti-6Al-4V that has undergone two passes at 1050°C, 1/s.

Table 15. Average flow stress, peak flow stress and strain, as well as critical stress and strain per pass, at 1050, 1/s.

Hit	Average flow stress (MPa)	Peak flow stress (σ_p)(MPa)	Critical flow stress (σ_c)	Peak Strain(ε_p)	Critical Strain (ε_c)
1	72	96	91	0.14	0.0058
2	65	62	58	0.45	0.18
3	66	65	62	0.91	0.36

Table 16. Volume fractions of α grains with each pass at 1050°C, 10/s.

Hit	Volume fraction of α grains (%)	Standard deviation
1	0	-
2	2	0.57
3	6	2.5

4.2.8 Deformation at 1050°C, 10/s

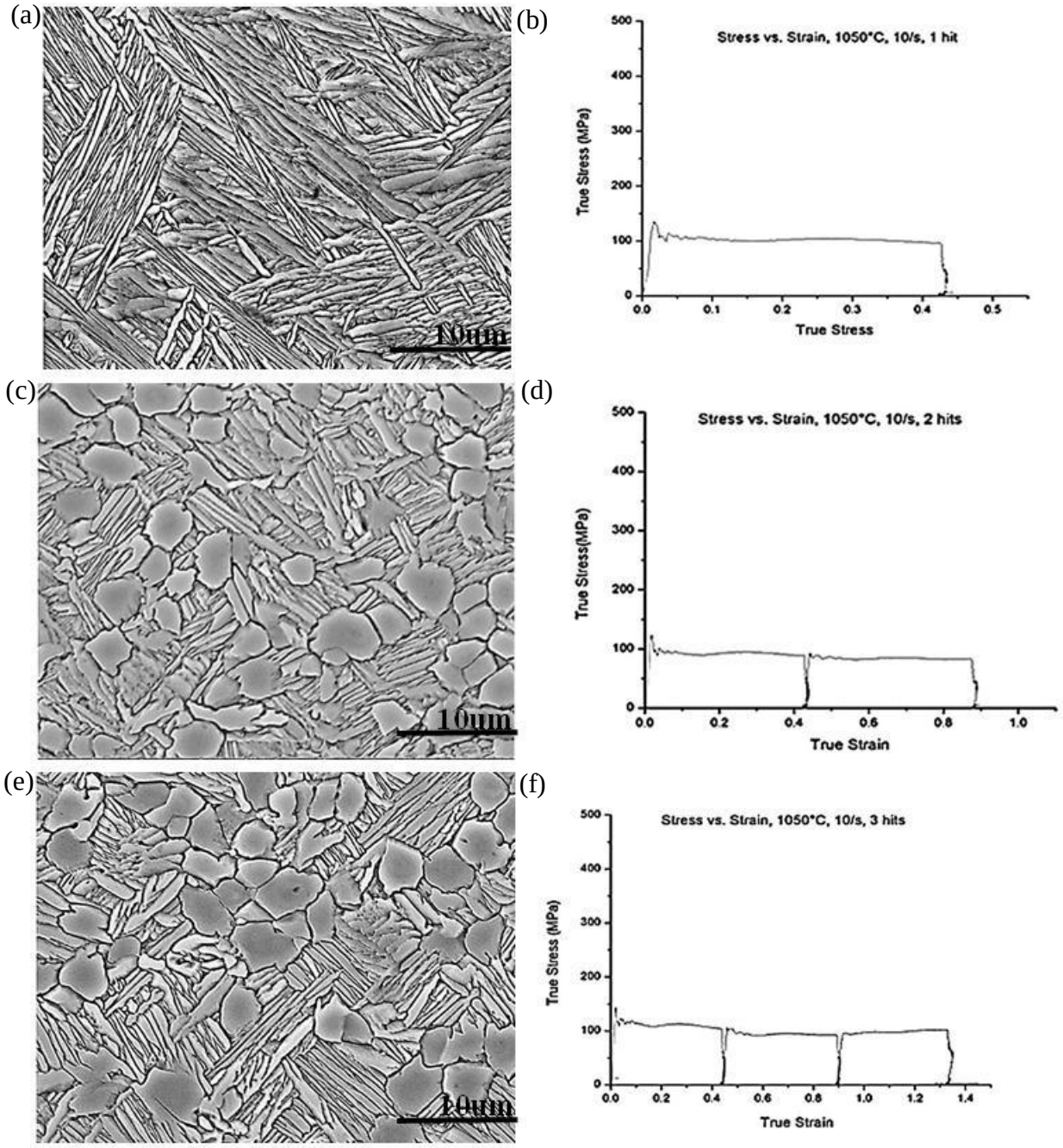

Figure 39. The microstructures (a)-(e) and true stress-true strain curves (b)-(f), depicting flow stress behaviour of Ti-6Al-4V after one, two and three hits at 1050°C, 10/s.

At 1050°C, using a strain rate of 10/s, a single pass resulted in a lamellar microstructure with Widmanstätten morphology [**Figure 39** (a)] and this was confirmed using EDS analysis for solute partioning. As in the case of uniaxial compression at 950°C, 10/s, instability was seen at the onset of deformation at the first pass and was due to difficulty in initiating dislocation movement at a high strain rate. After two successive passes at 1050°C, 10/s the microstructure is shown in [**Figure 39** (c)] and is bimodal. The phase transformation from β to α was more extensive compared to that at 1050°C, 1/s and this was due to the high strain rate used. The microstructure of Ti-6Al-4V after three passes is shown in [**Figure 39** (e)]. Unlike the time-temperature graph seen during uniaxial compression at 950°C, 10/s [**Figure 34**], the time-temperature at 1050°C, 10/s [Figure 40] displays no temperature fluctuations throughout the three passes. Therefore, the SIT of β phase into equiaxed α phase could be concluded to be a microstructural phenomenon.

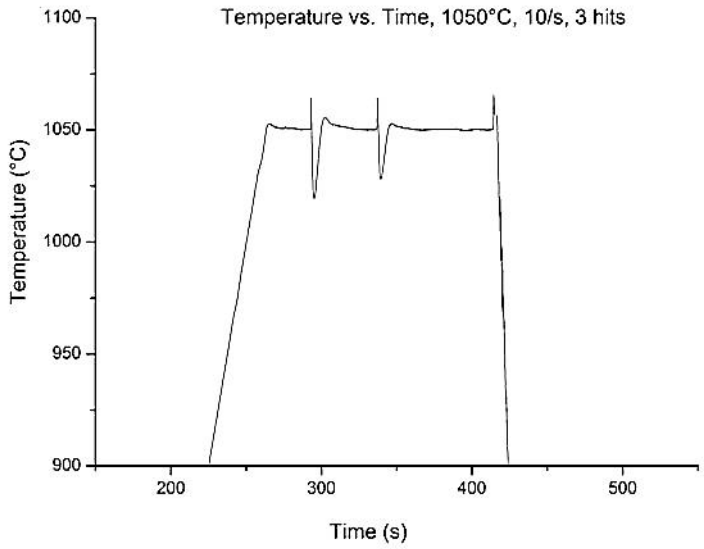

Figure 40. Temperature-time graph after three hits at 1050°C, 10/s.

Calculation of the volume fraction of equiaxed α grains revealed a slight difference in the volume fraction between hit two and hit three, increasing from 23% to 26% [**Table 18**]. In **Table 17**, the flow stress at each pass during hot deformation at 1050°C, 10/s is seen to decrease

because of the grain growth that occurred during both the 44s and 77s interpass times. True stress-true strain curves [**Figure 39 (**b)-(f)] reveal that the flow stress depicted steady state behaviour, which was initiated at the first pass.

Table 17. Average flow stress, peak flow stress and strain, as well as critical stress and strain per pass at 1050, 10/s.

Hit	Average flow stress (MPa)	Peak flow stress (σ_p)(MPa)	Critical flow stress (σ_c)	Peak Strain(ε_p)	Critical Strain (ε_c)
1	104	143	135	0.02	0.008
2	95	105	100	0.46	0.18
3	90	96	91	0.93	0.37

Table 18. Volume fractions of equiaxed α grains with each pass at 1050°C, 10/s.

Hit	Volume fraction of α grains (%)	Standard deviation
1	0	-
2	23	1.09
3	26	1.63

4.2.9 Summary

The microstructures after one hit at strain rates of 1 and 10/s are similar, consisting of α_w. With further strain imparted on these samples, the microstructures deviated from one another at the second and third hits: the microstructure after two and three hits at 10/s was bimodal, whereas that at 1/s, although containing some equiaxed α was still Widmanstätten. A strain rate of 10/s raised the extent of SIT upon air quenching, through the increase in the number of sites for nucleation and growth of equiaxed α grains. In the graph displayed in **Figure 41**, it can be seen that the average flow stress values at 10/s were higher than those at 1/s, although marginally so. Since the ductile β phase was the main constituent of the microstructure, the strain rate did not

impact so largely on the flow stress. Furthermore, the flow stress values decreased with each subsequent pass, following inter-annealing, and this was due to grain growth during the interpass times at 1/s and at 10/s.

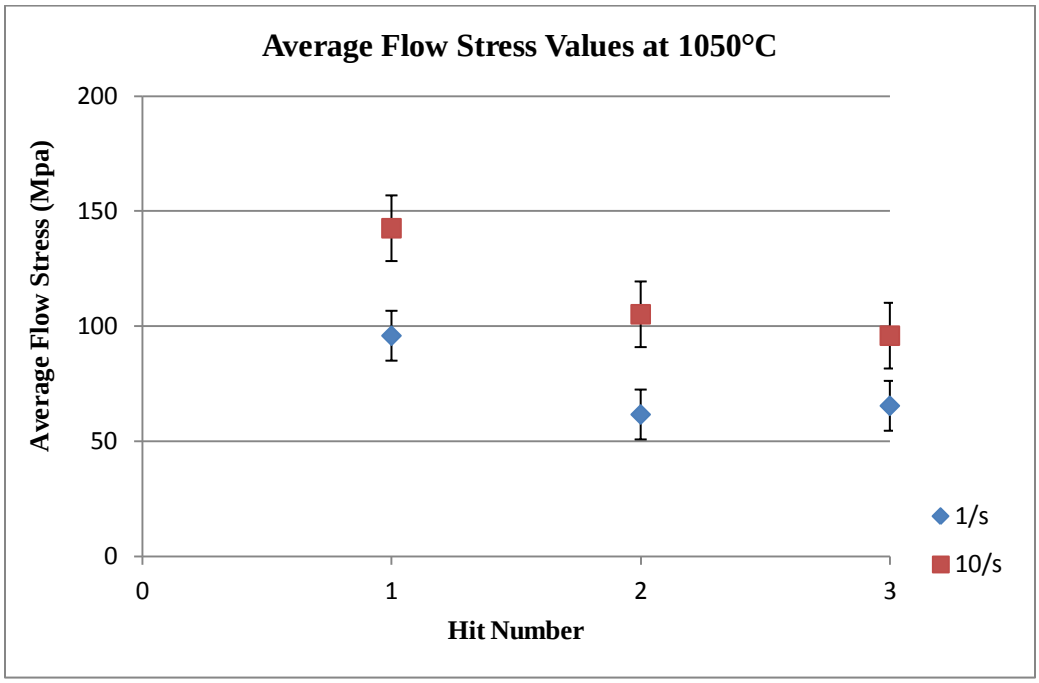

Figure 41. Graph of average flow stress values against pass number at 1050°C, 1/s and 10/s.

Table 19. The volume fraction of equiaxed α grains at 1050°C at either 1/s or 10/s.

Strain rate(/s)	Pass	Volume fraction of α grains (%)	Strain Rate(/s)	Pass	Volume fraction of α grains (%)
1	1	-	10	1	-
	2	2		2	23
	3	6		3	26

4.3 Influence of Temperature and Strain on Microstructure Evolution

4.3.1 Single Pass Deformation

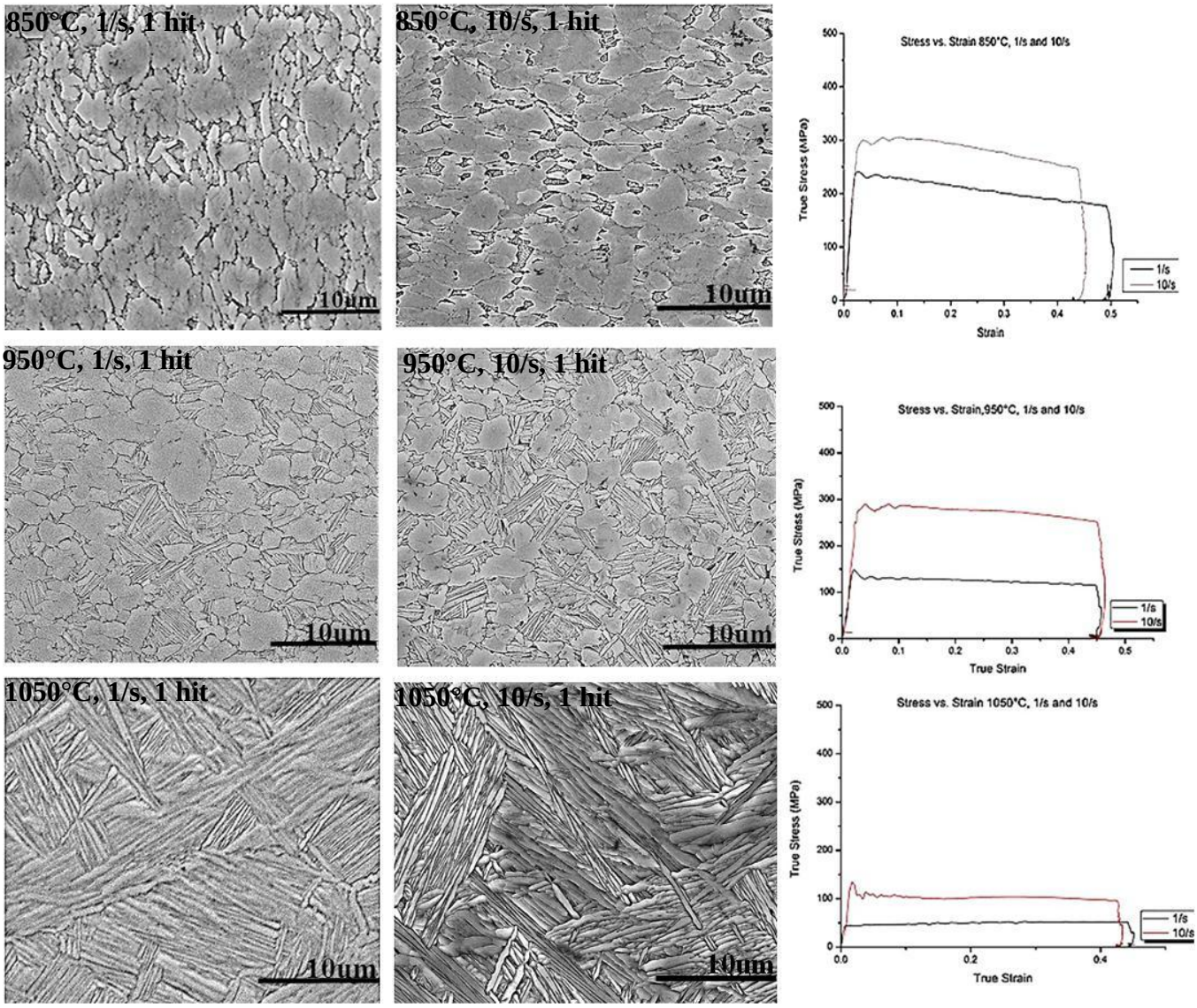

Figure 42. Micrographs of samples deformed at 850°C, 950°C,1050°C, 1/s or 10/s. True stress-true strain curves (a), (b) and (c) of samples that have undergone a single compression at either 1/s or 10/s.

After one hit at both 1/s and 10/s, the microstructures were of a similar morphology: deformed α grains at 850°C, bimodal at 950°C and Widmanstätten α-β lamellae at 1050°C. **Figure 42** (a-c), as well as **Table 20**,shows that the flow stress increased with strain rate if the temperature was

kept constant, whilst the flow stress decreased with an increase in temperature, a trend in agreement with that of other researchers[24,54]. Furthermore, at 850°C, the strain rate used affected the restoration mechanisms that took place within the microstructure during deformation, with evidence of recrystallisation at1/s vs. recovery at 10/s.While both microstructures were bimodal after deformation at 950°C, that of the sample compressed at 10/s had a higher volume fraction of lamellar α in contrast to its 1/s counterpart. This was a result of temperature fluctuations at that strain rate which might have resulted in adiabatic heating. Ti-6Al-4V, being a poor conductor is unable to dissipate heat when the strain rate is increased. Consequently, the temperature of the sample was higher than 950°C and the volume of the β phase increased. On quenching of the sample, the β phase transformed into α_w .

Table 20. Average flow stress values of Ti-6Al-4V after one hit.

Temperature	**Strain rate**	**Average flow stress (MPa)**
850°C	1	251
	10	313
950°C	1	201
	10	265
1050°C	1	72
	10	104

4.3.2 Influence of Interpass Time on Microstructure Evolution (Three-Pass Deformation Sequence)

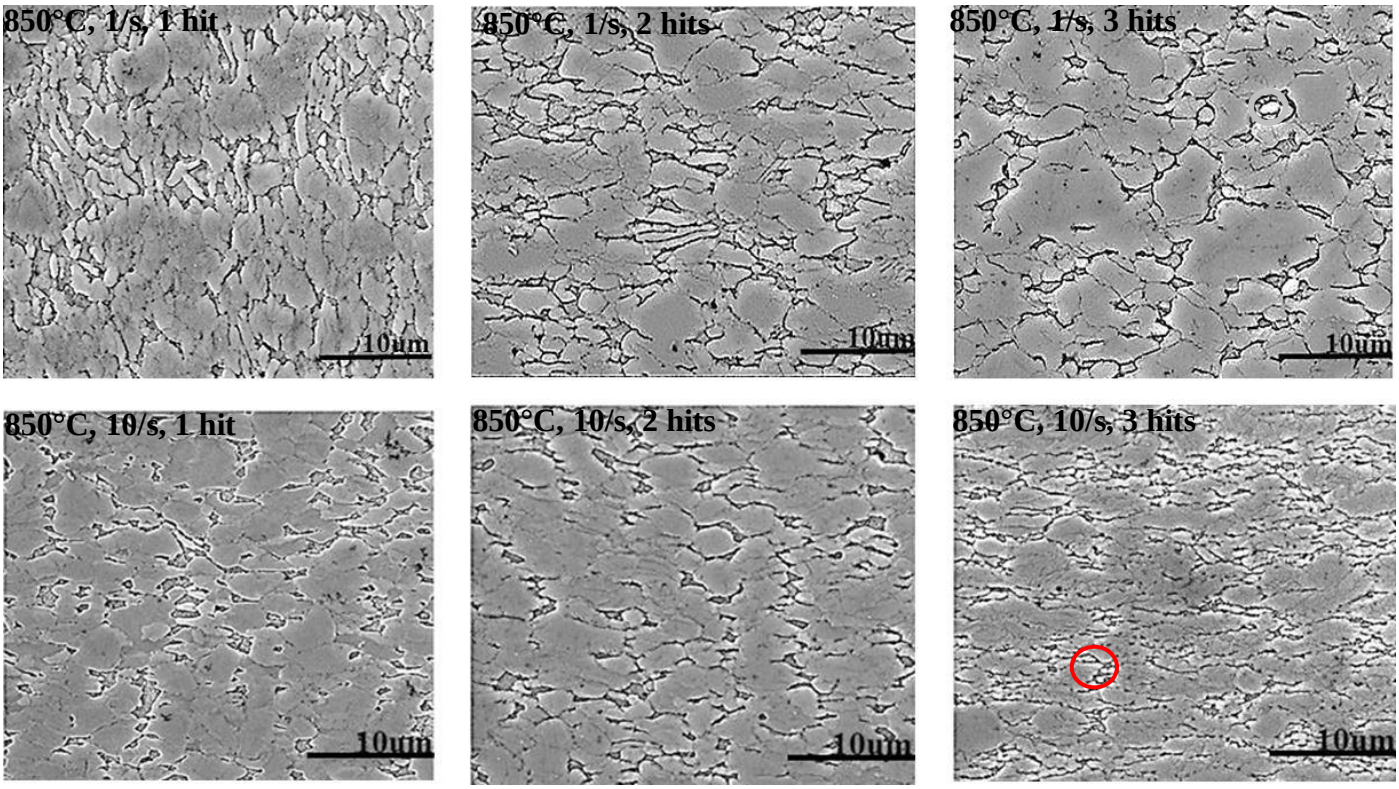

Figure 43. Micrographs of samples deformed at 850°C 1/s or 10/s after one, two and three hits. Recrystallised grains (circled) after three hits at 850°C, 10/s.

In **Figure 43**, it can be observed that after one hit at 850°C, 1/s, the microstructure consisted of deformed α grains. Following interpass times of 324s and 712s and their subsequent corresponding deformations, the microstructure still consisted of deformed grains and recrystallised grains, which had formed during deformation of the alloy, were also discernible. The influence of the interpass times at this temperature and strain rate was such that the deformed grains, having accrued dislocations during deformation, expended stored energy within the microstructure through static recrystallisation. Grain growth then proceeded and this resulted in the flow stress decreasing at the subsequent passes [**Figure 27** (b-f)]. At the same temperature but higher strain rate, the microstructure after one hit was similar to that obtained after one hit at 1/s. After an interpass time of 44s, following the first deformation and preceding the next, the microstructure, too, consisted of coarse, deformed grains, although in this instance, recrystallised

grains were not discernible This means that during the interpass time recrystallisation and grain growth took place bringing about the coarsening [**Figure 43**, two hits]. The sample was again held at temperature for 77s after the second hit. The grains, after this inter-anneal, were still heavily deformed. The resultant microstructure at 850°C, 10/s after one, two or three hits was affected by the strain rate, which resulted in a non-uniform distribution of strain. Thus, when the sample was annealed between passes, only the portions of the microstructure where the strain concentration was at its highest, recrystallised. Consequently, recrystallisation was heterogeneous (circled grains in **Figure 43**, three hits).

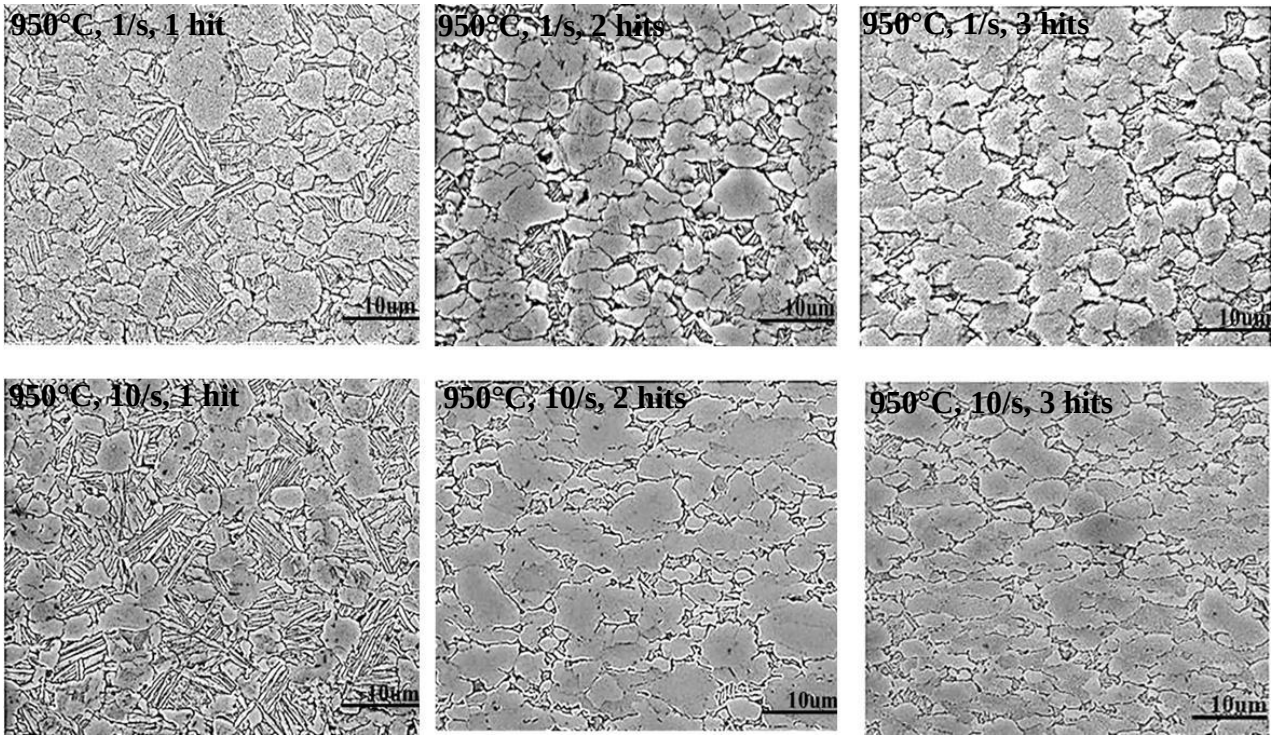

Figure 44. Micrographs of samples deformed at 950°C 1/s or 10/s after one, two and three hits.

The microstructure after one pass at 950°C, 1/s or 10/s was bimodal and evolved only when further strain had been imparted [**Figure 44**]. **Table 21** shows that the volume fraction of equiaxed α grains increased from 41.5% to 65% after two hits and then to 68% after three hits at 10/s. Conversely, the volume fraction of equiaxed α grains increased from 55% to 62.5% after two hits and then to 67% after three consecutive hits at 1/s. Although the final volume fraction of equiaxed α grains at either strain rate was similar after three successive hits, the interpass times

of 44s and 77s at 950°C, 10/s, resulted in a higher SIT of β phase into equiaxed α grains. This was evidenced by the 23.5% increase in equiaxed α grains from hit one to two at 10/s, compared to the 7.5% increase at 1/s. The SIT of β phase was enhanced, because the use of a higher strain rate generated a high density of dislocations. These not only served as nucleation sites for equiaxed α grains within the β phase, but also increased the stored energy that was the driving force for this transformation. The use of annealing times between passes at either strain rate allowed not just for the nucleation and growth of α grains via a strain induced phase transformation, but also for grain growth. This was evidenced by the fact that at 1/s and 10/s, coarse α grains were present in the final microstructure, although those observed in the microstructure at 10/s, while coarse, were deformed.

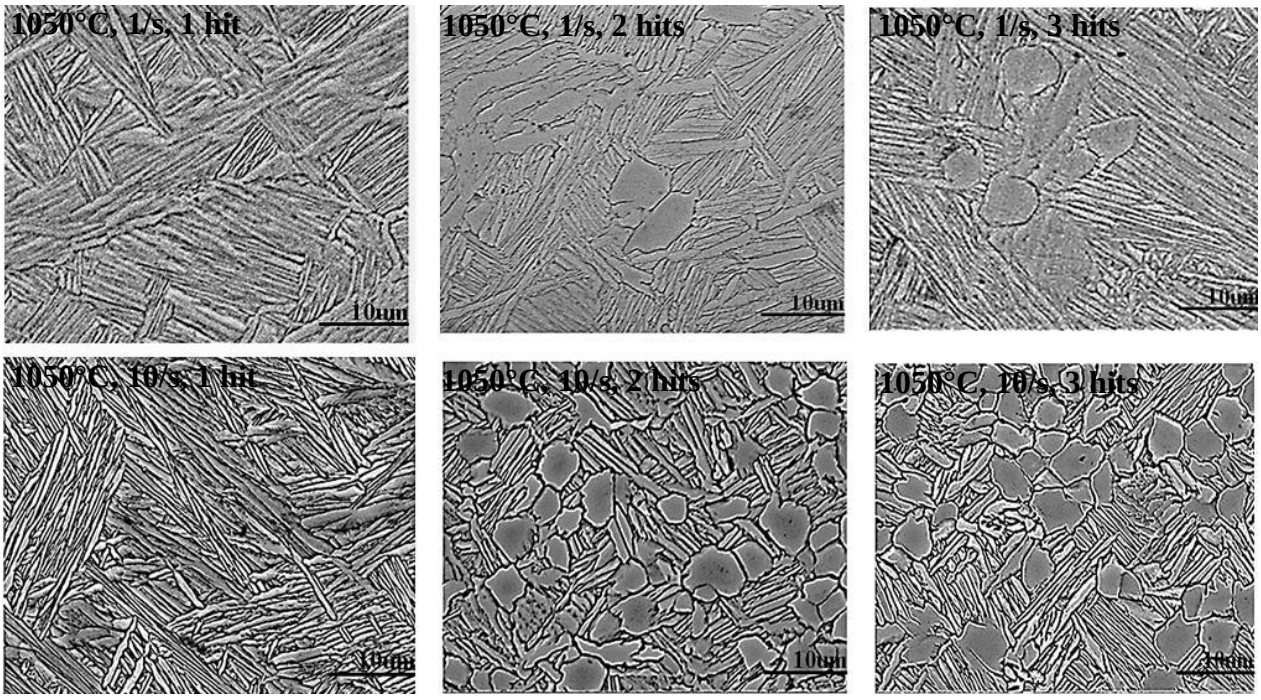

Figure 45. Micrographs of samples deformed at 1050°C, 1/s or 10/s after one, two and three hits.

At 1050°C, after one hit using a 1/s or 10s strain rate the microstructure was comprised of Widmanstätten α-β lamellae [**Figure 45**]. An interpass time of 324s at 1/s resulted in equiaxed α forming within the microstructure, although this was less than that observed at 950°C, 1/s (2 % at 1050°C,1/s vs. 55% at 950°C,1/s). The dislocations generated at this temperature were lessened by the low strain rate and so the sites upon which equiaxed α could nucleate from β

phase during quenching were reduced. In addition, the high temperature meant that dislocations were annihilated faster. Consequently, during this inter-anneal period, growth of β grains occurred, rather than an SIT. The scenario was the same when the sample was annealed for 712s after the second hit. However, when a 10/s strain rate was used, the volume fraction of equiaxed α increased, but this was less than that seen after the sample had undergone three hits at 950°C, 10/s [**Table 21**]. Despite dislocations being eradicated faster because of the elevated temperature, the strain rate was still sufficiently high to ensure that the dislocation density was sufficient for the nucleation of globular α phase.

Table 21. Volume fraction of equiaxed α grains at 950°C at, 1/s or 10/s and 1050°C, 10/s.

Temperature (°C)	**Strain rate (/s)**	**Pass**	**Volume fraction of α grains (%)**	**Strain rate (/s)**	**Pass**	**Volume fraction of α grains (%)**
950	1	1	55	10	1	41.5
		2	62.5		2	65
		3	67		3	68
1050	1	1	0	10	1	0
		2	2		2	23
		3	7		3	26

4.4 Analysis of Variance (ANOVA) and the Taguchi Method

ANOVA yielded the results presented in [**Table 22**, **Table 24**,**Table 26**]. From these tables it was observed that the calculated F value for temperature was higher than that of strain rate for all passes. This meant that temperature was the more influential parameter towards microstructural restoration and the finding was in accordance with those of Babu *et al*.[53]. The results of the Taguchi method [**Table 23**,**Table 25**, **Table 27**] show that the optimum processing parameters for the rolling of Ti-6Al-4V, using a three pass schedule were a temperature of 1050°C and a strain rate of 1/s. However, based on microstructural analysis, these parameters yielded a microstructure that was mainly Widmanstätten α-β lamellae the shortcoming of the microstructure being its low ductility. However, where creep resistance was a necessity, a lamellar microstructure would serve[4,55]. For purposes where the metal was still to be deformed and ductility required, the microstructure obtained after three passes at a temperature of 950°C and a strain rate of 10/s would suit as it was comprised of a recrystallised α microstructure that was malleable[32]. The microstructure obtained after three passes at 850°C, 10/s was unsuitable due to the highly deformed grains that arose following compression. This microstructure, as well as the non-uniform distribution of recrystallised grains, would yield a similarly heterogeneous microstructure, even if a post deformation heat treatment were to be carried out. Furthermore, the high force required to deform the alloy using these parameters would require a large amount of energy, which is not cost-effective. Whilst hot compression using a strain rate of 1/s at the same temperature did not present the same challenges as 10/s, there was the matter of coarse grains brought about by the use of long interpass times. This was, in fact, true of all samples deformed at 1/s for all deformation temperatures. A coarse-grained microstructure is, of course, unsuitable for industrial applications mainly as it is lacking in strength.

Table 22. ANOVA for flow stress after one pass.

Source of variation	F_{calc}	F_{crit}
°C	111.81	3.89
(s)	23.50	4.74

Table 23. S/N ratios after one pass.

	Strain Rate (/s)	Temperature (°C)	S/N ratio
1 pass	1	1	6.35E-05
	1	2	9.54E-05
	1	3	7.50E-04
	2	1	3.88E-05
	2	2	5.40E-05
	2	3	3.50E-04

Table 24. ANOVA for flow stress after two passes.

Source of variation	F_{calc}	F_{crit}
°C	107.55	3.89
(/s)	26.25	4.74

Table 25. S/N ratios after two passes.

	Strain Rate (/s)	Temperature (°C)	S/N ratio
2 passes	1	1	9.40E-05
	1	2	1.52E-04
	1	3	1.22 E-03
	2	1	6.81E-05
	2	2	7.00E-05
	2	3	4.74 E-04

Table 26. ANOVA for flow stress after three passes.

Source of variation	F_{calc}	F_{crit}
°C	56.64	3.89
(/s)	18.41	4.74

Table 27. S/N ratios after three passes.

	Strain Rate(/s)	Temperature (°C)	S/N
	1	1	1.23 E-04
3 passes	1	2	1.50 E-04
	1	3	8.45 E-04
	2	1	9.05E-05
	2	2	7.59E-05
	2	3	4.19 E-04

5. Summary

In this section, the main findings relating to the effect of the deformation parameters, temperature and strain rate on microstructural evolution, as well as on the flow stress of Ti-6Al-4V, are summarised.

5.1 Influence of Deformation Temperature on the Uniaxial Compression of Ti-6Al-4V

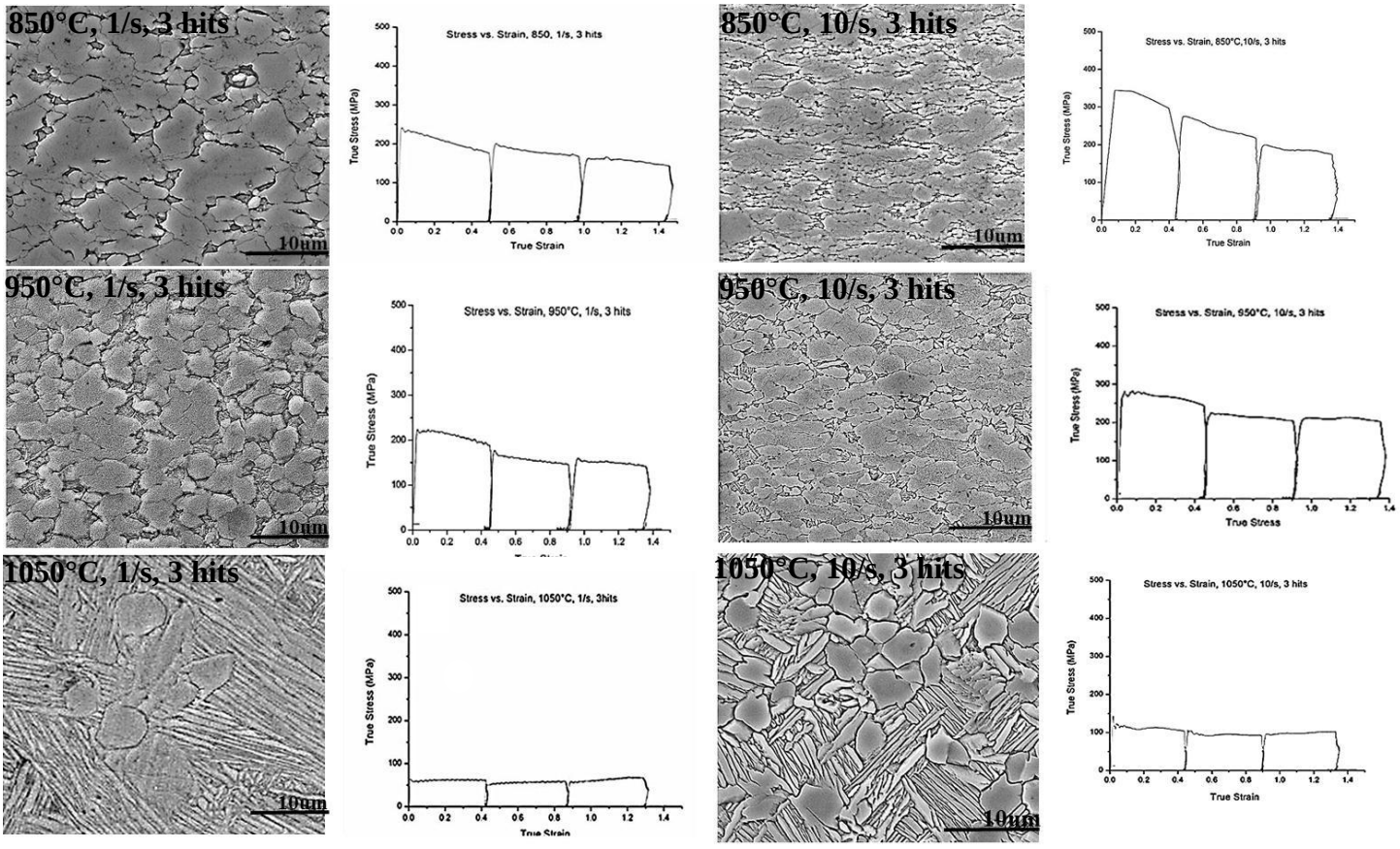

Figure 46. True stress-true strain curves (a)-(f) and corresponding microstructures of Ti-6Al-4V after three hits and test temperatures of either 850°C, 950°C or 1050°C, strain rates of 1/s or 10/s.

Figure 46 shows the true stress-true strain curves of Ti-6Al-4V samples, deformed using temperatures of 850 ° C, 950°C or 1050°C. It can be observed from **Figure 46** that the flow stress required to deform Ti-6Al-4V is reduced with an increase in temperature regardless of the strain rate, an observation that holds true for all passes. This is due to an increase in the volume

fraction of the ductile β phase from 20% at 850°C to 100% at temperatures above the T_β. A change of morphology from deformed α grains to bimodal to Widmanstätten after one hit is also a result of the presence of the β phase [**Figure 42**].

With an increase in temperature, the flow stress behaviour throughout the three passes also changes. At 950°C, flow softening is seen after the first two passes, indicating that a SIT has taken place during deformation. Thereafter, at the third pass, following the second anneal, steady state flow stress is observed once a critical strain of 0.431 has been reached [**Figure 46** (d), **Table 28**]. **Table 28** also shows that the critical strain rate is predictably at its lowest at 1050°C. Here, steady state flow stress is observed from the initial pass, where the critical strain is 0.00796, and is maintained throughout the three passes. Steady state flow stress at the highest deformation temperature is due to the enhanced climb and glide of dislocations, which in turn increases recrystallisation kinetics, with the result that the onset of recrystallisation is shifted to lower values[46]. Therefore, a higher deformation temperature experiences a greater extent of recrystallisation[56]. At the lower temperatures (850°C, 950°C), steady state flow stress only manifests at the third pass.

Table 28. Critical strain values for the onset of recrystallisation at 850°C, 950°C, and 1050°C, 1/s and 10/s.

Temperature (°C)	**Pass**	**Strain rate (/s)**	**Critical strain (σ_c)**	**Strain rate (/s)**	**Pass**	**Critical strain (ε_c)**
850	1	1	0.0104	10	1	0.067
	2		0.213		2	0.194
	3		0.448		3	0.392
950	1	1	0.012	10	1	0.031
	2		0.19		2	0.19
	3		0.39		3	0.42
1050	1	1	0.0058	10	1	0.0079
	2		0.18		2	0.18
	3		0.36		3	0.37

5.2 Influence of Strain Rate on the Uniaxial Compression of Ti-6Al-4V

In **Figure 46** (a)–(f) it can be seen that, for a given temperature, an increase in strain rate results in higher flow stress values[24]. **Table 28** shows that, with an increase in strain rate, the critical strain value required to initiate recrystallisation is also elevated. This behaviour is to be expected[57], because at high strain rates the high dislocation density leads to a decrease in the work hardening rate[58]. Consequently, the onset of recrystallisation is shifted to higher strain values[46].

However, the morphology of the microstructure remains the same after one pass, despite the strain rate used. That is, the microstructure consists of α grains after one pass at 850°C, 1/s or 10/s, is bimodal after one pass at 950°C, 1/s or 10/s, and Widmanstätten after one pass at 1050°C, 1/s. At the higher temperatures, such as, for example, at 1050°C, 10/s continued straining of the alloy transforms the microstructure from Widmanstätten to bimodal. This shows that morphological changes in the microstructure of Ti-6Al-4V can only be effected through further deformation of the alloy and the extent of the transformation enhanced by strain rate.

While the increase in strain rate does not alter the morphology of the microstructure after one pass, it does, nevertheless, lead to grain refinement at 950°C, 10/s [**Figure 48**]. Calculation of the α grain size, using the linear intercept method, yields a grain size of approximately 7.5uṃ for the sample deformed at 1/s, and 6.8.uṃ for the sample deformed at 10/s. Grain size refinement at this temperature is only detectable after one hit, since the grains become very deformed after subsequent passes at 950°C. At 1050°C, this is not possible because grain growth is very rapid, following dynamic recrystallisation. Furthermore, subsequent passes (one+two and one+two+three), using the higher strain rate, promoted the β to equiaxed α phase transformation at both 950 °C and 1050°C. This led to an increase in the volume fraction of α grains, as shown in **Figure 49**. A high strain rate brings about dislocation multiplication, thus increasing stored energy which acts as a driving force for phase transformation. The increase in dislocation density further serves to increase the sites for the nucleation of the equiaxed α phase.

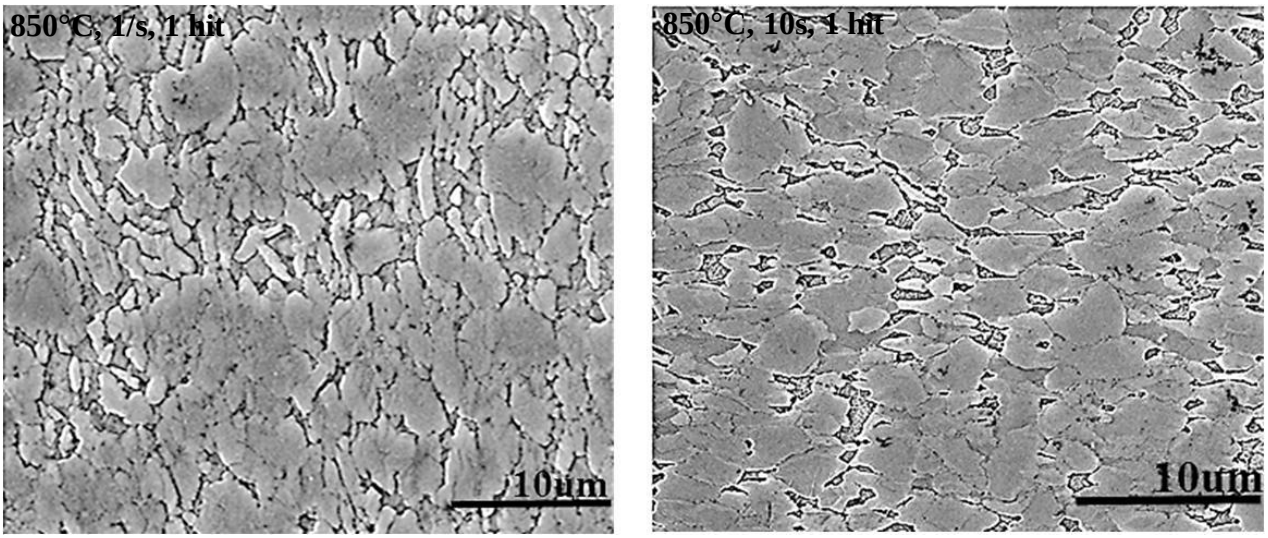

Figure 47. Uniaxial compression at 850°C, 1/s led to higher recrystallisation than at 850°C,10/s.

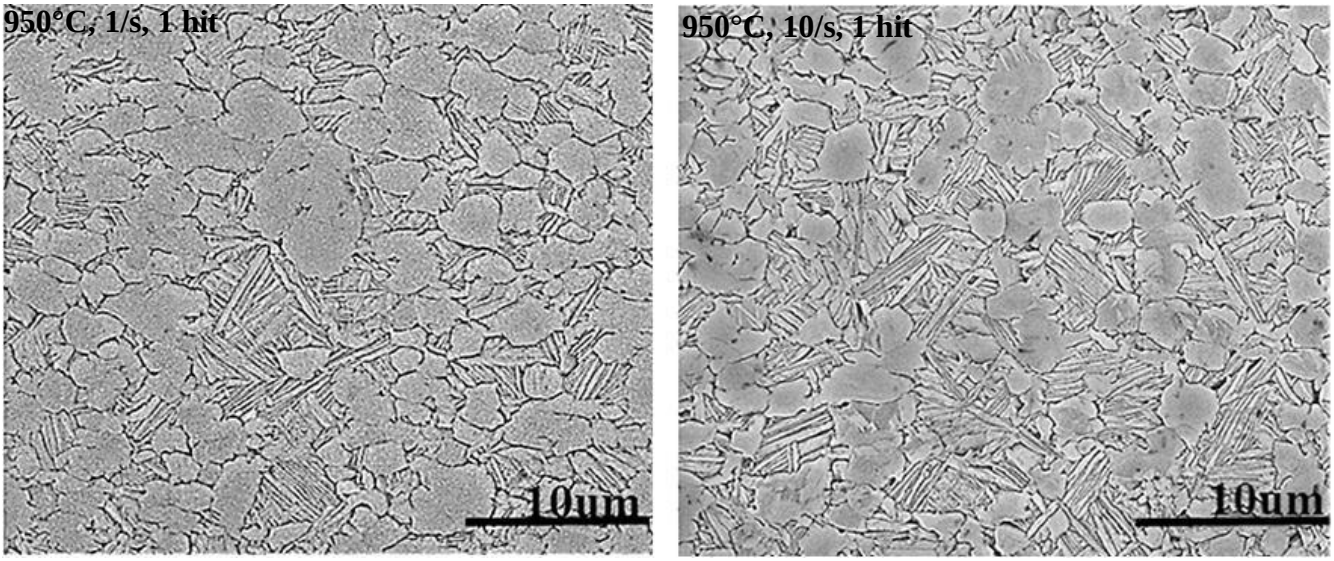

Figure 48. Micrographs showing the grain size refinement that occurred when a strain rate of 10/s was used, in comparison to when a strain rate of 1/s was used, at 950°C.

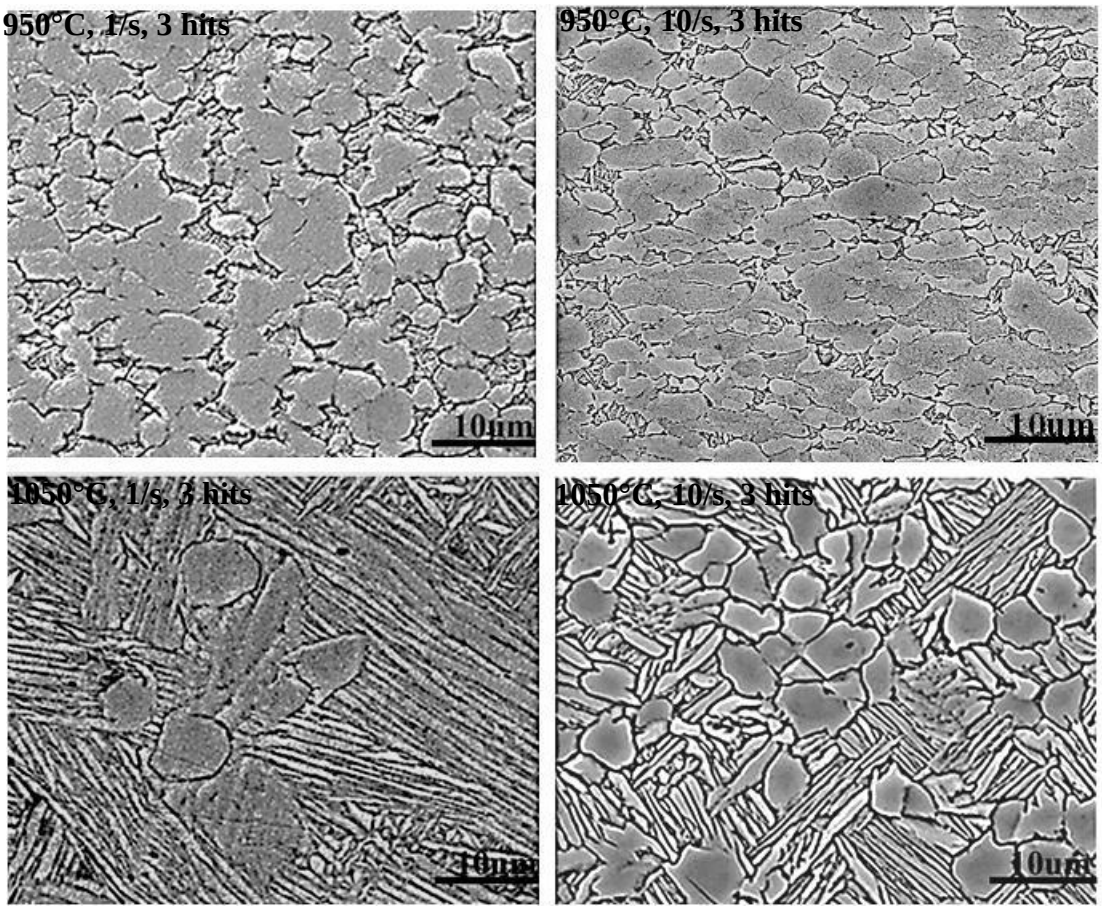

Figure 49. Micrographs of Ti-6Al-4V after three hits at 950°C, 1/s or 10/s and 1050°C, 1/s or 10/s.

That recrystallisation is more extensive at 1/s also manifests within the flow curves themselves. In **Figure 46** (a), (c) and (e), the flow stress curves all exhibit oscillatory behaviour and this is in line with observations by other researchers, where DRX has taken place during hot deformation of metals at low strain rates[6,44,46]. This oscillatory behaviour is indicative of cycles of recrystallisation starting and completing before being succeeded by other cycles, which then also initiate and reach completion. It is a mark of low strain rate, enabling diffusion of dislocations, and, as the strain rate is low, there is sufficient time for nucleation and growth of recrystallised grains. The oscillatory behaviour in the flow stress is no longer observed at all temperatures at the higher strain rate [**Figure 46** (b), (d) and (f)] because the higher strain rate does not provide sufficient time for cycles of recrystallisation to occur and reach completion. The various cycles of DRX are instead averaged out and thus present in a smooth line.

Cessation of deformation while at high temperature encourages static recrystallisation, as well as grain growth, during the time the sample is held at temperature. As the interpass time is linked to a corresponding strain rate, the extent of grain growth obviously increases, the longer the sample is annealed. This is especially observed in the microstructures of samples deformed at 850°C, 950°C and 1050°C, at a strain rate of 1/s, after interpass times of 324s and 712s.

6. Conclusions

- The multipass deformation of Ti-6Al-4V using a three-pass schedule, similar to that employed during steckel mill rolling, is feasible, as no defects, such as voids or cracks, occurred. There was also no fracture of the samples during the uniaxial compression tests. Moreover, the parameters used in this experiment were well within the range of those that can be used in a steckel mill.
- Microstructure evolution during this process was successfully assessed and subsequently characterised and it was seen that the deformations of temperature, strain rate and interpass time dramatically affect this evolution as follows:
- For every 100°C increase in temperature, the morphology of the microstructure evolved from equiaxed to bimodal and was Widmanstätten at the final test temperature of 1050°C.An increase in recrystallisation was also observed with an increase in temperature, with Ti-6Al-4V samples deformed at 1050°C being the most recrystallised. However, grain growth also occurred at this temperature. Finally, as the test temperature was increased, deformation of the alloy was made easier, as the increase brought about a decrease in the flow stress.
- The incidence of a strain-induced phase transformation increased with an increase in strain rate at 950°C and 1050°C. At a strain rate of 1/s, where the interpass times were higher than those used at 10/s, growth of dynamically recystallised grains occurred, resulting in coarse, deformed microstructures.
- ANOVA shows that temperature is the more influential parameter with regards to microstructural restoration. The Taguchi method identified the temperature of 1050°C and strain rate of 1/s as the optimum processing parameters, using a “higher the better” signal-to-noise ratio. However, the choice of microstructure would be dependent on the application for which the material was to be used. For those requiring high creep strength, the microstructure acquired after uniaxial compression at 1050°C, 1/s would suit, whilst for applications requiring ductility, the microstructure obtained after three passes at 950°C, 10/s would be more suitable.

7. Recommendations

With regards to further work in this project, the following is recommended:

- Post deformation heat treatment should be conducted to determine the influence of a post deformation heat treatment on the further microstructure evolution of the samples that have undergone multiple deformations.
- The multipass deformation of Ti-6Al-4V at strain rates higher than 10/s and temperatures above 850°C should also be investigated as these will also lower the interpass times used. By lowering the interpass times, the process would be much faster and this would increase the appeal of using a steckel mill to produce Ti-6Al-4V sheet material.
- Plane strain compression (PSC) of Ti-6Al-4V, using a multipass schedule may also be carried out in the Gleeble 3800, to investigate the texture effects this might have on the alloy used in this study.
- To investigate the extent of recrystallisation, transmission electron microscopy (TEM) may be done on the deformed samples.

8. References

1. Seong, S., Younossi, O. & Goldsmith, B. W. Titanium: Industrial Base, Price Trends, and Technology Initiatives. 128 (2009).

2. Knutsen, R. D. & Parker, S.A. Analysis of Microstructure Evolution during Steckel Mill Rolling of AISI304 Stainless Steel. *ISIJ Int.* **48,** 200–207 (2008).

3. Sellars, C. M. Recrystallization of Metals during Hot Deformation. *Philos. Trans. R. Soc. A Math. Phys. Eng. Sci.* **288,** 147–158 (1978).

4. Luterjing, G., Williams, J. C. *Titanium*. (Springer, 2003).

5. Leyens, C. & Peters, M. *Titanium and Titanium Alloys: fundamentals and applications*. (Weilly-VCH, 2003).

6. Seshacharyulu, T., Medeiros, S. C., Frazier, W. G. & Prasad, Y. V. R. K. Hot working of commercial Ti–6Al–4V with an equiaxed α–β microstructure: materials modeling considerations. *Mater. Sci. Eng. A* **284,** 184–194 (2000).

7. Donachie, M. J. *Titanium: A Technical Guide*. (ASM International, 2000).

8. Kelly, S. M. *Thermal and Microstructure Modeling of Metal Deposition Process with Application to Ti-6Al-4V. PhD Thesis VIrginia Polytechnic Institute and State University* (2004).

9. Malinov, S., Sha, W., Guo, Z., Tang, C. . & Long, a. . Synchrotron X-ray diffraction study of the phase transformations in titanium alloys. *Mater. Charact.* **48,** 279–295 (2002).

10. Gil Mur, F. X., Rodríguez, D. & Planell, J. a. *Influence of tempering temperature and time on the α'-Ti-6Al-4V martensite*. *Journal of Alloys and Compounds* **234,** (1996).

11. Sun, Z., Guo, S. & Yang, H. Nucleation and growth mechanism of ??-lamellae of Ti alloy TA15 cooling from an ?? + ?? phase field. *Acta Mater.* **61,** 2057–2064 (2013).

12. Koul, M. K. Transformation and Deformation studies in Titanium Alloys. (Massachusetts Institute of Technology, 1968).

13. Ahmed, T. & Rack, H. J. *Phase transformations during cooling in α+β titanium alloys*. *Materials Science and Engineering: A* **243,** (1998).

14. Matsumoto, H. *et al. Room-temperature ductility of Ti-6Al-4V alloy with α' martensite microstructure*. *Materials Science and Engineering A* **528,** (Elsevier B.V., 2011).

15. Ray, K. & Ray, K. A STUDY ON HOT ROLLING OF CP TITANIUM BY B . Tech .(Hons .), Indian Institute of Technology , Kharagpur , India A THESIS SUBMITTED IN PARTIAL FULFILLMENT OF THE REQUIREMENTS FOR THE DEGREE OF MASTERS OF APPLIED SCIENCE (DEPARTMENT OF METALS AND MATERIAL. (1996).

16. Semiatin, S. L. & Bieler, T. R. Effect of texture and slip mode on the anisotropy of plastic flow and flow softening during hot working of Ti-6Al-4V. *Metall. Mater. Trans. A* **32,** 1787–1799 (2001).

17. Williams, J. Thermo-mechanical processing of high-performance Ti alloys: recent progress and future needs. *J. Mater. Process. Technol.* **117,** 370–373 (2001).

18. Humphreys, F. J. & Hatherly, M. *Recrystallization and related annealing phenomena*. *Acta Metallurgica et Materialia* (2004). doi:10.1016/B978-008044164-1/50005-0

19. Seshacharyulu, T., Medeiros, S. C., Frazier, W. G. & Prasad, Y. V. R. K. Microstructural mechanisms during hot working of commercial grade Ti-6Al-4V with lamellar starting structure. *Mater. Sci. Eng. A* **325,** 112–125 (2002).

20. Guo-zheng, Q. in *Recent Developments in the Study of Recrystallization* (ed. Wilson, P.) 62–87 (intech, 2013).

21. Mcqueen, H. J. & Tegart, W. J. M. The deformation of metals at high temperatures. *Sci. Am.* **232,** 116–125 (1975).

22. McQueen, H. . & Ryan, N. . Constitutive analysis in hot working. *Mater. Sci. Eng. A* **322,** 43–63 (2002).

23. Andersen, I., Grong, Ø. & Ryum, N. Analytical modelling of grain growth in metals and alloys in the presence of growing and dissolving precipitates--II. Abnormal grain growth. *Acta Metall. Mater.* **43,** 2689–2700 (1995).

24. Ding, R., Guo, Z. X. & Wilson, a. Microstructural evolution of a Ti–6Al–4V alloy during thermomechanical processing. *Mater. Sci. Eng. A* **327,** 233–245 (2002).

25. Tamirisakandala, S., Vedam, B. V. & Bhat, R. B. Recent Advances in the Deformation Processing of Titanium Alloys. *J. Mater. Eng. Perform.* **12,** 661–673 (2003).

26. Prasad, Y. V. R. K. & Seshacharyulu, T. Processing maps for hot working of titanium alloys. *Mater. Sci. Eng. A* **243,** 82–88 (1998).

27. Semiatin, S. L., Seetharaman, V. & Weiss, I. The thermomechanical processing of alpha/beta titanium alloys. *Jom* **49,** 33–39 (1997).

28. Zherebtsov, S., Murzinova, M., Salishchev, G. & Semiatin, S. L. Spheroidization of the lamellar microstructure in Ti-6Al-4V alloy during warm deformation and annealing. *Acta Mater.* **59,** 4138–4150 (2011).

29. Margolin, H. Cohen, P. Titanium ’80. *Titan. ’80 Sci. Technol.* 1555–1561 (1980).

30. Zherebtsov, S., Murzinova, M., Salishchev, G. & Semiatin, S. L. Spheroidization of the lamellar microstructure in Ti-6Al-4V alloy during warm deformation and annealing. *Acta Mater.* **59,** 4138–4150 (2011).

31. Benedetti, M. and Fontanari, V. The effect of Bi-modal and lamellar microstructures of the Ti6Al4V behaviour of fatigue cracks emanating from edge-notches. *Fatigue Fract. Eng. Mater. Struct.* **27,** 1073– 1089 (2004).

32. Park, C. H., Son, Y. Il & Lee, C. S. Constitutive analysis of compressive deformation behavior of ELI-grade Ti-6Al-4V with different microstructures. *J. Mater. Sci.* **47,** 3115–

3124 (2012).

33. Weng, B. S. X. & Thomas, J. E. Modern Steckel Mills Introduction : Basic Physics of the Steckel Mill Analysis of the Conventional Steckel Mill Layout. 1–9 (2015).

34. No Title. Available at: www.ssab.com/Products--Services/About-SSAB/Steel-making-process/Processing/Sheet-steel.

35. No Title. Available at: www.tifast.com/ingots.asp. (Accessed: 12th April 2015)

36. Babu, J., Dutta, A. & Kumaraswamy, A. Experimental Studies on Effect of Temperature and Strain Rate on Deformation Behaviour of Ti-6Al-4V Using Taguchi Method. *Procedia Mater. Sci.* **6,** 1121–1130 (2014).

37. Mccormick, F. J. & Huang, C. L. Strain Distribution Within Compressed Circular Cylinders. 497–501

38. Banerjee, J. K. Barreling of Solid Cylinders Under Axial Compression.pdf. *J. Mater. Technol.* **107,** 138 (1985).

39. Davis, J. . in Metals Handbook Ninth Edition: Volume 8 Mechanical (ASM International, 1985).

40. Prasad, Y. V. R. K., Seshacharyulu, T., Medeiros, S. C. & Frazier, W. G. Influence of oxygen content on the forging response of equiaxed (??+??) preform of Ti-6Al-4V: Commercial vs. ELI grade. *J. Mater. Process. Technol.* **108,** 320–327 (2001).

41. Vanderhasten, M., Rabet, L. & Verlinden, B. AME high temperature deformation of Ti-6Al-4V at low strain rate. *Metalurgija* **11,** (2005).

42. Salishchev, G.A., Galeyev, R.M., Valiakhmetov, O.R., Safiullin,R.V., Lutfullin, R.Y., Senkov, O.N., Froes, F.H., Karibyshev, O. A. Development of Ti-6Al-4V sheet with low temperature superplastic properties. *J. Mater. Process. Technol.* **116,** 265–268 (2001).

43. Bai, Q. *et al.* Modelling of dominant softening mechanisms for Ti-6Al-4V in steady state hot forming conditions. *Mater. Sci. Eng. A* **559,** 352–358 (2013).

44. Humphreys, F. J. & Hatherly, M. *Recrystallization and related annealing phenomena*. *Acta Metallurgica et Materialia* (2004). doi:10.1016/B978-008044164-1/50005-0

45. Wang, K., Luan, B.F., Li, M.Q., Liu, Q. Phase Dependent Restoartion Mechanisms of TC8 Titanium Alloy during Hot Compression in the Two Phase Region. *Mater. Sci. Eng.* **89,** 1–6 (2015).

46. Guo-zheng, Q. Characterization for Dynamic Recrystallization Kinetics Based on Stress-Strain Curves. *Recent Dev. Study Recryst.* 61 – 64 (2013). doi:10.5772/54285

47. Honarmandi, P. & Aghaie-Khafri, M. Hot Deformation Behavior of Ti-6Al-4V Alloy in β Phase Field and Low Strain Rate. *Metallogr. Microstruct. Anal.* **2,** (2013).

48. Abbasi, S. M. & Momeni, a. Effect of hot working and post-deformation heat treatment on microstructure and tensile properties of Ti-6Al-4V alloy. *Trans. Nonferrous Met. Soc. China* **21,** 1728–1734 (2011).

49. Park, N. K., Yeom, J. T. & Na, Y. S. Characterization of deformation stability in hot forging of conventional Ti-6Al-4V using processing maps. *J. Mater. Process. Technol.* **130-131,** 540–545 (2002).

50. He, L., Dehghan-Manshadi, A. & Dippenaar, R. J. The evolution of microstructure of Ti-6Al-4V alloy during concurrent hot deformation and phase transformation. *Mater. Sci. Eng. A* **549,** 163–167 (2012).

51. Dehghan-Manshadi, A., Dippenar, R. J. Strain-induced phase transformation during thermo-mechanical processing of titanium alloys. *Mater. Sci. Eng. A* **552,** 451–456 (2012).

52. Kun, Q. I. N., Li-ming, Y. & Shi-sheng, H. U. Mechanism of Strain Rate Effect Based on Dislocation Theory. **26,** 1–4 (2009).

53. Babu, J., Dutta, A. & Kumaraswamy, A. Experimental Studies on Effect of Temperature and Strain Rate on Deformation Behaviour of Ti-6Al-4V Using Taguchi Method. *Procedia Mater. Sci.* **6,** 1121–1130 (2014).

54. Mukerjee, K. K. A critical review of the mechanics of metal rolling; its application to the design of hot strip mills. (Montreal Universty, Canada, 1973).

55. Kim, J. Y., Park, K.-T., Shim, I. O. & Hong, S. H. Globularization Behavior of ELI Grade Ti-6Al-4V Alloy during Non-Isothermal Multi-Step Forging. *Mater. Trans.* **49,** 215–223 (2008).

56. Honarmandi, P. & Aghaie-Khafri, M. Hot Deformation Behavior of Ti–6Al–4V Alloy in β Phase Field and Low Strain Rate. *Metallogr. Microstruct. Anal.* **2,** 13–20 (2012).

57. Lukac, P. (Charles U. in *Adavnced Light Alloys and Composites* (ed. Ciach, R.) 291–298 (Kluwer Academic Publishers, 1997).

58. Lee, W. S., Shyu, J. C. & Chiou, S. T. Effect of strain rate on impact response and dislocation substructure of 6061-T6 aluminum alloy. *Scr. Mater.* **42,** 51–56 (1999).